

THESIS

DEVELOPMENT AND TESTING OF A MULTIPLEXING SYSTEM FOR
LASER IGNITION OF LARGE BORE NATURAL GAS ENGINES

Submitted by

Adam Robert Reynolds

Department of Mechanical Engineering

In partial fulfillment of the requirements

For the Degree of Master of Science

Colorado State University

Fort Collins, Colorado

Fall 2011

Master's Committee:

Advisor: Azer Yalin

Bryan Willson

Jacob Roberts

This work is licensed under the Creative Commons Attribution-Noncommercial-Share Alike 3.0 United States License. To view a copy of this license, visit <http://creativecommons.org/licenses/by-nc-sa/3.0/us/> or send a letter to Creative Commons, 171 Second Street, Suite 300, San Francisco, California, 94105, USA.

ABSTRACT

DEVELOPMENT AND TESTING OF A MULTIPLEXING SYSTEM FOR LASER IGNITION OF LARGE BORE NATURAL GAS ENGINES

Conventional electric spark plugs present a hindrance to the continuing goals of higher efficiency and reduced emissions for large-bore natural gas engines. In order to achieve these goals, higher compression ratios and higher air-to-fuel ratios must be achieved relative to those currently allowed by conventional spark plugs. Laser ignition has been shown to work farther into the lean limit, and contrary to conventional electric spark plugs, laser sparks are *easier* to produce at higher pressures. Laser ignition has also been shown to reduce NO_x emissions. This work presents efforts to design, build, and test a single-laser-to-multiple-cylinders multiplexed laser ignition system for use with a large bore natural gas engine. A fiber based laser delivery system was found to work for laser ignition on the bench-top. Results of bench top tests are presented.

TABLE OF CONTENTS

1	Introduction	1
1.1	Laser Ignition	2
1.1.1	Basics	2
1.1.2	Benefits to Gas Engines	3
1.2	Practical Systems – Open vs. Closed Systems	6
1.2.1	Fiber Delivery of Laser Ignition Light	8
1.2.1.1	Hollow Core Fibers	11
1.2.1.2	Fiber Laser	12
1.2.1.3	Solid Core Fiber	13
1.3	Need for Multiplexed Fiber Delivery	13
1.4	Problem Statement	15
2	Preliminary Development and Testing	16
2.1	Methods of Multiplexing	16
2.1.1	Solid-state Multiplexing Methods	16
2.1.1.1	Electro-Optic Modulators	16
2.1.1.2	Acousto-Optic Modulators	19
2.1.1.3	Summary of EOM & AOM Approaches	19
2.1.2	Mechanical Multiplexing Methods	19
2.2	Initial Galvanometer Test	24
3	Multiplexer Design	28
3.1	Design Constraints	28
3.2	Simulations	29

3.3	Design Overview	31
4	Spark Plug Design	37
4.1	Introduction	37
4.2	Design Overview	37
4.3	Post Design-Phase Changes	43
5	Multiplexer Tests	45
5.1	Bench-top Tests	45
5.1.1	Setup	45
5.1.2	Bench-top Control System	46
5.1.3	Pressure Chamber	46
5.1.4	Energy Transmission	50
5.1.5	Beam Characterization	51
5.1.6	Sparking Tests	52
6	Conclusion	54
6.1	Summary	54
6.2	Outlook	56
A-1	Multiplexer technical drawings	69
A-2	Sparkplug technical drawings	80
A-3	Pressure chamber technical drawings	85

1 Introduction

The ongoing effort to increase efficiency while reducing emissions of large-bore natural gas spark-ignition engines presents a set of unique problems. The efficiency and power output of an engine may be increased by increasing the compression ratio or boost. But this eventually produces auto-ignition, or knock, in an engine. In order to reduce knock, the air-to-fuel ratio must be increased (i.e., the engine must be run lean-burning). Eventually, two limiting factors are reached: the ‘lean-limit,’ where there is not enough fuel in the mix for a conventional spark plug to properly ignite; and the declining performance of electric spark plugs as gas pressures increase, which requires higher spark plug voltages and leads to markedly increased spark plug wear and therefore more frequent replacement and downtime.

Laser ignition has been shown to work farther into the lean-limit than conventional spark plugs, thus reducing the NO_x produced by the engine [1–3], and a laser produced spark is more easily formed as pressures are increased (whereas a conventionally produced electric spark is harder to form with increased pressure) [1, 2, 4–6]. These results indicate that laser ignition is a promising alternative to spark plugs in large-bore natural gas engines, allowing for higher engine efficiency and lower emissions.

The work described in this thesis was performed at the Colorado State University Engines and Energy Conversion Laboratory, where a working laser ignition system was developed and tested on a Caterpillar G3516C engine with one laser multiplexed into multiple cylinders through hollow core fiber optics.

1.1 Laser Ignition

1.1.1 Basics

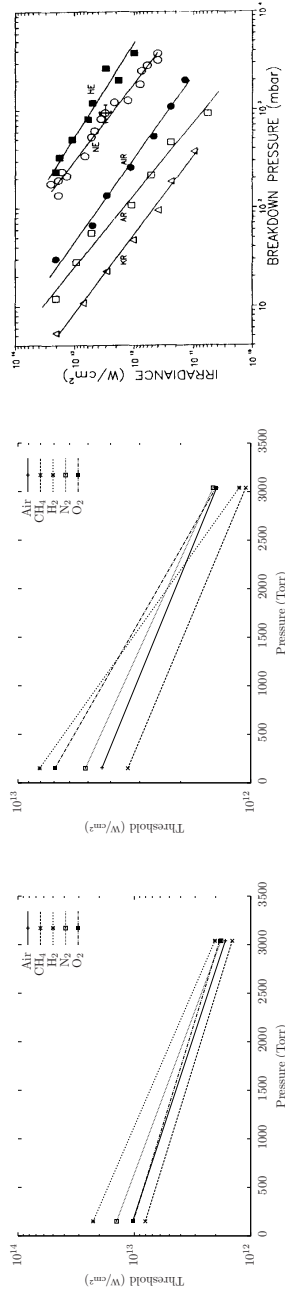
Laser ignition results from a gas breakdown that is induced by a beam of laser light. When a sufficiently powerful pulse of laser light is focused to a small spot, the gas within the focal spot is ionized, producing a spark, and the resulting plasma kernel is sufficient to ignite a combustible gaseous mixture [7]. It has been found that ignition of lean mixtures requires a pulse energy of about 10–20 mJ [2], called the *Minimum Ignition Energy*, any less than this and the laser may produce a spark but the mixture will not be ignited. In the application of laser ignition, this ionization of gas is primarily accomplished through the electron cascade process [7], whereby initial free electrons created by multi-photon ionization absorb photons. When the electrons reach sufficient energy, they ionize other molecules in the gas, leading to the generation of even more free electrons. The resulting cascade causes the breakdown of the gas. The onset of this process shows a pressure dependence of approximately $P^{-0.4}$ for 1064 nm light [7], which is important to the application of laser ignition to internal combustion engines since these engines exhibit considerably higher than atmospheric pressures during the ignition phase of their operation.

For nanosecond scale pulsed lasers, the intensity needed for laser-induced breakdown varies with the type of gas, pressure, and laser wavelength. Reported thresholds for air at atmospheric pressure are in the range of $\sim 1000 \text{ GW/cm}^2$ [7–10]. Figures 1.1 and 1.2 shows some of the reported laser-induced breakdown thresholds. As can be seen from these graphs, the laser-induced breakdown threshold depends not only on the pressure, but also on the laser wavelength [7, 9–11]. Breakdown may be achieved by focusing the laser beam to a small spot a few mm to a few cm in front of a lens, where the spark occurs at the focal region in an approximately cylindrical shape coaxial with the beam and lens axes, as in Figure 1.3. Focusing optics also play a part in

determining the maximum beam-waist focal intensity necessary for breakdown [12].

1.1.2 Benefits to Gas Engines

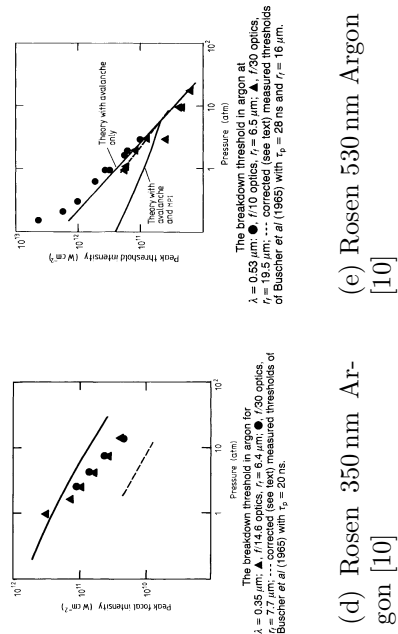
Laser ignition of engines provides a number of potential benefits over conventional electric spark plug ignition. First, initial flame propagation is faster because the flame kernel is protected by positioning the spark away from the cylinder walls [1, 2, 4, 5, 11, 13–15]. Spark plug electrodes are also eliminated, which prevents flame kernel quenching. As a result, ignition delay and 0 - 10% mass burn duration is shorter, and maximum cylinder pressure can be higher, and reached faster, resulting in greater fuel efficiency. Figure 1.4(a) shows how the cylinder pressure rises faster, Figure 1.4(b) shows that fuel is burned quicker, and Figure 1.4(c) shows the heat is released sooner for laser ignition versus spark ignition. Second, higher air-to-fuel ratios can be reached using laser ignition, thus extending the lean limit [1, 2, 4, 5, 12, 15, 16], which leads to lower combustion temperatures, lower NO_x generated, and higher thermal efficiency [1, 3, 4, 7, 15, 16]. Figure 1.4(d) shows the extension of the lean limit for laser ignition, and Figure 1.4(e) shows reduced NO_x generation for laser ignition. Third, higher compression ratios are possible with laser ignition, because the energy required to generate a spark *decreases* as pressure increases, which is the opposite of what happens with a conventional electric spark. This process particularly increases engine efficiency when coupled with the extended lean limit sparking that laser ignition provides [1, 6, 15, 16]. Fourth, due to the ready-made optical pathway provided by a laser ignition system, light may be pulled out of the cylinder (during or after sparking) in order to perform real-time optical diagnostics of the flame, which could help in closer loop control of (tuning) the engine while it is running [12]. Fifth, the lack of conventional electric spark plugs in a laser ignition system potentially extends the operational time of the system and may reduce long-term costs given the



(a) Phuoc 532 nm [7]

(b) Phuoc 1064 nm [7]

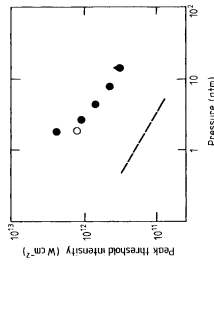
(c) Turcu 248 nm [9]



(d) Rosen 350 nm Ar-gon [10]

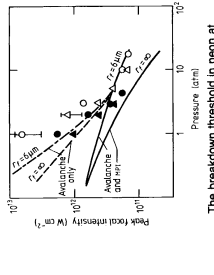
(e) Rosen 530 nm Argon [10]

Figure 1.1: Laser breakdown thresholds measured by various researchers.



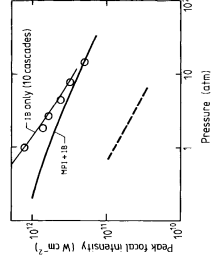
The breakdown threshold in neon at $\lambda = 0.35 \mu\text{m}$: \circ , red glow $f/14.8$ optics, \bullet , white flash with $f/14.8$ ($f/25.7$) optics and $r = 6.4 \mu\text{m}$ ($11.1 \mu\text{m}$). --- data of Alcock *et al* (1972) with $r = 27 \mu\text{m}$.

(a) Rosen 350 nm Neon [10]



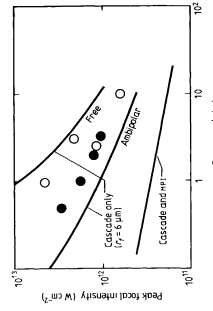
The breakdown threshold in neon at $\lambda = 0.53 \mu\text{m}$. Experiments: \circ , pure neon with $f/10$ optics, \bullet , neon seeded with 1000 ppm of xylene, \blacktriangle , $f/15$ optics $r = 10 \mu\text{m}$. Theory: --- avalanche and MPI, --- MPI only.

(b) Rosen 530 nm Neon [10]



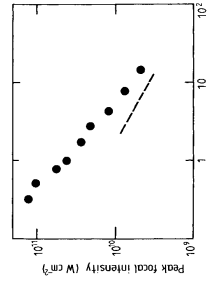
The breakdown threshold in nitrogen at $\lambda = 0.35 \mu\text{m}$: \circ , $f/10$ optics, $r = 4.3 \mu\text{m}$. ---, measurements of Alcock *et al* (1972), $f/14$, $r = 27 \mu\text{m}$; ---, theory for $r = 4.3 \mu\text{m}$.

(c) Rosen 350 nm Nitrogen [10]



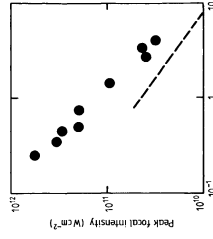
The breakdown threshold in nitrogen at $\lambda = 0.53 \mu\text{m}$: \circ , pure nitrogen, \bullet , nitrogen seeded with 1000 ppm of xylene, $f/10$ optics, $r = 6.5 \mu\text{m}$; ---, theory for $r = 6 \mu\text{m}$.

(d) Rosen 530 nm Nitrogen [10]



The breakdown threshold in xenon at $\lambda = 0.35 \mu\text{m}$: \bullet , $f/30$ optics with $r = 13 \mu\text{m}$; --- data of Buscher *et al* (1965) with $r = 7.7 \mu\text{m}$.

(e) Rosen 350 nm Xenon [10]



The measured breakdown threshold in xenon at $\lambda = 0.53 \mu\text{m}$. --- data of Buscher *et al* (1965) with $r_p = 28 \text{ ns}$.

(f) Rosen 530 nm Xenon [10]

Figure 1.2: Laser breakdown thresholds measured by various researchers.

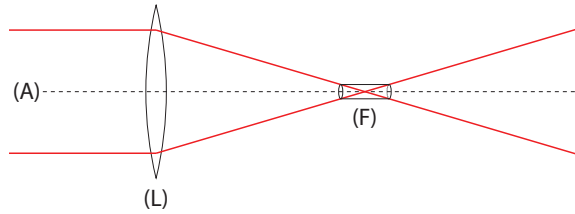


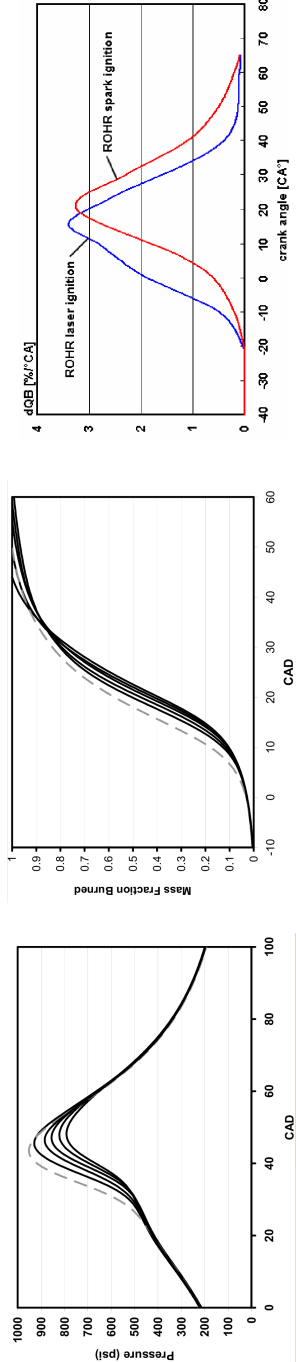
Figure 1.3: Schematic diagram of the lens setup to form a spark with a laser. The laser beam extents are shown as solid lines, with the beam axis following the dotted line (A). The beam is focused by the lens (L) to the focal point at (F), where an approximately cylindrical plasma spark is formed.

price trajectories of pulsed lasers [1]. Other benefits of laser ignition include very precise spark timing [1, 4], and the possibility of multi-point ignition wherein many sparks may be generated within the cylinder simultaneously [1, 16–19].

1.2 Practical Systems – Open vs. Closed Systems

Any practical laser ignition system needs to deliver the laser light into the combustion chamber in a robust and reliable way. Much laboratory research has focused on using an *open beam path approach*, where mirrors are used to direct the laser beam into the cylinder through the open air. Unfortunately, this method has several disadvantages when one considers a practical on-engine laser ignition system. First is the fact that this system exhibits poor alignment stability in the face of thermal drift and vibration. Second is the problem of contamination of the mirror and lens surfaces due to the presence of vapors and/or particulates, resulting in decreased optical transmission. Finally, the open beam path is a danger to technicians and others working on the engine who are unfamiliar with the safety requirements of working with high-power lasers. Therefore, some means of mitigating these disadvantages must be found.

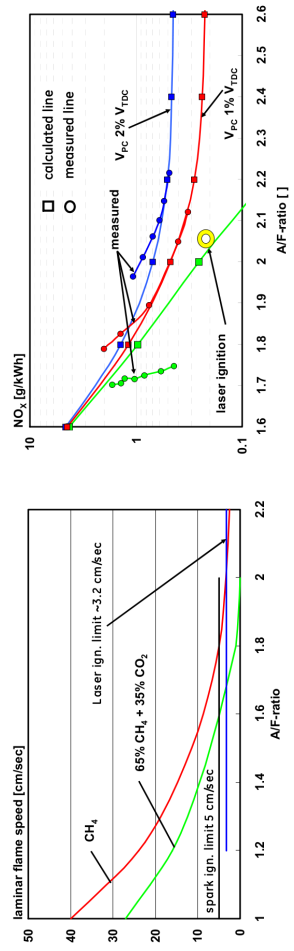
One way of accomplishing this is to attach the laser to the combustion chamber, such that it has a direct line of sight into the chamber through any needed focusing optics. This alleviates the problem of misalignment due to thermal drift, vibration,



(a) Pressure vs. crank angle degree (CAD) for laser (dotted) and spark ignited (solid) cylinders. [12]

(b) Mass fraction burned vs. crank angle degree (CAD) for laser (dotted) and spark ignited (solid) cylinders. [12]

(c) The heat release of laser vs. spark ignition, showing that laser ignition has faster ignition than spark. [16]



(d) Extension of the lean limit by laser ignition. [15]

(e) Comparison of NO_x generated for direct ignition, pre-chamber ignition, and laser ignition, showing reduced NO_x for laser ignition. [15]

Figure 1.4: Benefits of laser ignition to gas engines.

and long beam paths. However, in this approach one laser cannot be distributed to multiple cylinders, rather one laser is required for each cylinder. Further, available space and the thermal load on the laser source due to being in close proximity to the engine are also of concern. Nevertheless, several groups have developed compact laser sources for precisely this one laser per cylinder application [20–24].

To ensure maximum flexibility, and to take advantage of the ability to distribute one laser source to multiple cylinders, a *closed path, fiber delivered laser ignition system* is preferred. This method is not only safer (because the beam is fully enclosed), it also reduces the problems associated with vibration, heat, and contamination. The most straightforward and simple delivery method in the closed-path system is to transmit the laser ignition pulse directly to the combustion chamber by fiber, with the required focusing optics placed after the fiber exit. However, the fiber is then subject to burdensome optical power requirements due to the required breakdown and ignition conditions of laser ignition. Alternately, the laser pump light may be delivered via fiber to a gain medium located adjacent to the combustion chamber, which then produces the laser ignition pulse. This method places lower requirements on the fiber optics due to the lower peak power of the pump light, but is more complex and expensive due to the need for a separate laser gain element for each cylinder [21].

1.2.1 Fiber Delivery of Laser Ignition Light

Due to its simplicity and potential for a low cost system, fiber delivery of laser ignition light has been the focus of research at Colorado State University. A basic schematic of the setup to form a spark with fiber delivery is shown in Figure 1.5. The laser is launched into the fiber via launch optics (generally a positive lens). The focusing optics (one or more positive lenses) are placed downstream of the fiber exit. The two primary problems associated with the fiber delivery of ignition light are the fiber

intensity damage threshold, and the fiber output beam quality characterized by the value M^2 , defined as [25]:

$$M^2 = \pi \frac{\theta w_0}{\lambda} \quad (1.1)$$

where θ is the half-angle beam divergence, λ is the wavelength, and w_0 is the radius at the beam waist.

In order to form a spark, a sufficiently high power pulse must be delivered, with a good enough beam quality to achieve a small enough spot that will result in the required gas breakdown that produces the spark.

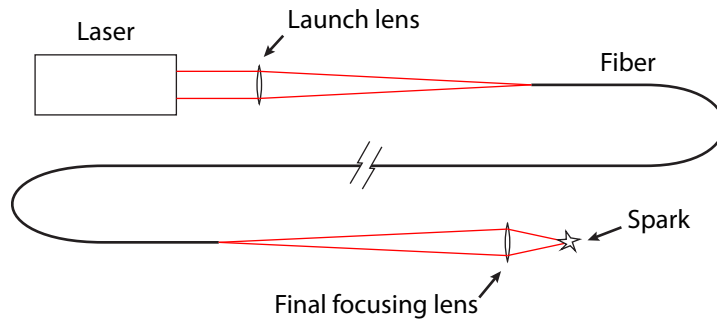


Figure 1.5: Diagram showing the schematic setup for fiber delivery of laser light to produce a spark. The beam is focused with the launch lens into the fiber. When it exits the fiber, the beam is focused by the final lens to a point, where it forms a spark.

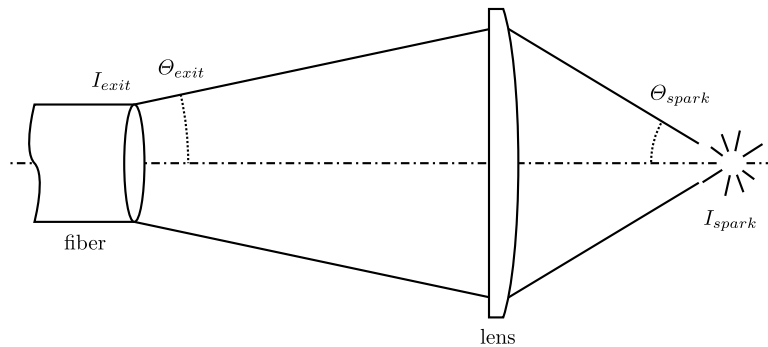


Figure 1.6: Diagram showing the elements of a fiber spark setup needed to calculate the FOM.

To evaluate the suitability of various fiber optic candidates, a Figure of Merit (FOM) is used [12]. The FOM allows an estimation of the achievable focused intensity (i.e., the intensity at the desired spark location), based on the fiber output parameters. The equation to calculate the FOM for a specific fiber, given published or measured values of fiber output (exit) quantities, is [12]:

$$FOM \equiv \frac{I_{spark}}{\theta_{spark}^2} = \frac{I_{exit}}{\theta_{exit}^2} \quad (1.2)$$

where I_{spark} is the post-fiber focused intensity achievable, θ_{spark} is the convergence angle of the light at the spark location (limited by lens selection and hardware space constraints), I_{exit} is the maximum intensity achievable at the fiber exit face, and θ_{exit} is the divergence angle of the light exiting the fiber (see Figure 1.6). In order to achieve spark formation, the minimum value of the Figure of Merit must be [12]:

$$FOM_{min} = 1400 \pm 800 \text{ GW/cm}^2\text{rad}^2 \quad (1.3)$$

For solid core silica fibers with a typical $\theta_{exit} \approx 0.11$ rad, and a maximum $I_{exit} \approx 3 \text{ GW/cm}^2$, $FOM \approx 250 \text{ GW/cm}^2\text{rad}^2$, significantly less than the FOM_{min} above. Use of solid fibers is discussed further in Sections 1.2.1.3 and 6.2.

On the other hand, coated hollow fibers can have significantly higher FOM ($FOM \approx 8900 \text{ GW/cm}^2\text{rad}^2$) [12]. CSU researchers have shown the use of coated hollow core fibers to produce sparks at atmospheric pressure [8, 26]. These fibers have also been used at Colorado State University to ignite a single cylinder of a natural gas engine [12]. The fibers are described in more detail in the next section.

1.2.1.1 Hollow Core Fibers

In order to achieve laser induced sparking at atmospheric pressure or at engine motored conditions, fibers in a closed-path laser ignition system must be capable of carrying the necessary energy load and they must produce high quality beams. Cyclic olefin polymer-coated silver hollow fibers which meet these criteria have been developed and produced at Tohoku University in Japan. Figure 1.7 shows a schematic of these fibers [26–28]. Originally developed for carrying mid-infrared laser light such as CO₂ and Er:YAG ($\lambda = 10.6\ \mu\text{m}$ and $2.94\ \mu\text{m}$ respectively), these fibers may also be coated for various other wavelengths, including the fundamental Nd:YAG wavelength of 1064 nm. Typically, they have inner diameters of 500–1000 μm , and may be flexed, but they experience increased loss and beam quality degradation as curvature is increased.

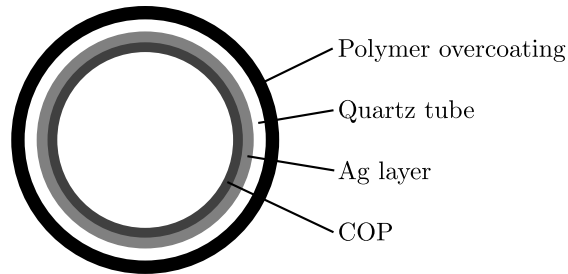


Figure 1.7: Diagram of the layers in a cyclic olefin polymer-coated silver hollow fiber: Polymer overcoating, Quartz tube, Silver (Ag) layer, and COP (cyclic olefin polymer) layer.

Experiments at Colorado State University have been conducted to determine the properties of these hollow core fibers with respect to spark formation and laser ignition [26]. Results show that in order to achieve low exit angular divergence, a low launch angle is required, for example, for a hollow core fiber of diameter 1 [mm], conditions of $\theta_{launch} = 7\ \text{mrad}$ and $w_{launch} = 254\ \mu\text{m}$ using a 50 cm focal length lens have been shown to be appropriate. This results in an output $M^2 \approx 11$ corresponding to a beam exit

divergence of 11 mrad. Damage to the fiber occurs when the reflective optical coating threshold is reached, about 1 GW/cm^2 [26–30], which is similar to that for solid core fibers. Additionally, the entry face of the fibers tend to spark in atmospheric air, so a helium purge must be used or vacuum must be pulled through the fiber to reduce this occurrence. As mentioned previously, sparking has been achieved for straight fibers, while bent fibers exhibit increased loss as well as increased M^2 . Recent work at CSU has shown spark delivery with 2 m fibers bent at 90 degrees at an elevated pressure of 15.2 bar.

In other experiments, these fibers have been successfully used to run a single cylinder of a 6-cylinder Waukesha VGF natural gas engine [12]. The laser and launch optics were mounted with vibration damping vertically above the engine. The hollow fiber led straight into an optical spark plug, which contained the focusing optics as well as a window into the combustion chamber. For the duration of the tests 100% ignition reliability was shown for the laser ignited cylinder, with the remaining cylinders ignited by the conventional spark plugs.

1.2.1.2 Fiber Laser

A fiber laser integrates the laser gain medium directly into a fiber optic. This eliminates the possibility of fiber surface damage when launching a laser beam into a fiber, since the laser light is generated within the fiber. Furthermore, high energy pulsed fiber lasers are undergoing rapid development, and recent experiments at the University of Michigan have shown an ability to produce sparks in atmospheric pressure air at the output of a fiber laser [31]. These tests employed a multi-stage fiber amplification system with an $80 \mu\text{m}$ core diameter Yb-doped fiber, with an output beam quality of $M^2 = 1.5$. When set up to produce 0.7 ns long pulses of 2.4 mJ, and with appropriate focusing optics at the output, sparking was achieved at 50 Hz

in atmospheric pressure air.

Fiber lasers are thought to be a very promising technology for laser ignition due to their high output beam quality coupled with the advantages derived from launching light directly into the fiber. Further, their low cost and simplicity makes them attractive for industrial applications. However, while the fiber laser produces excellent beam quality, higher energy levels must be achieved in order to yield robust ignition. Most researchers believe that fiber lasers will achieve the required energies in the near future. Other strategies based on combining multiple spatial or temporal pulses are also possible.

1.2.1.3 Solid Core Fiber

While use of solid core fibers remains challenging, recent research has shown some possible approaches. El-Rabii and Gaborel have recently achieved spark formation in air at elevated pressures with solid core silica fibers, aided by the fact that laser breakdown intensity threshold decreases with increased pressure [32]. Additionally, they were able to ignite atomized droplets of *n*-heptane in air through a solid core optical fiber at spark energies of 30 mJ.

Recent research at CSU has been successful in producing sparks through large clad step-index fibers at atmospheric pressure at energies of 3 to 4 mJ (using 10 ns Q-switched pulses). This energy is lower than the required 15 to 20 mJ needed for ignition, but further research is being conducted into increasing the energy delivered to the spark [33,34]. This work is discussed further in Section 6.2.

1.3 Need for Multiplexed Fiber Delivery

While the most direct approach to accomplish laser ignition in engines is that of a direct-mounted laser per cylinder, this method is very expensive for multi-cylinder

engines due to the high cost of high power lasers, even in production quantities. A method by which one laser may be used to ignite multiple cylinders, called multiplexing, is the desirable alternative.

A multiplexing system with fiber-delivered laser ignition light is desirable over an open beam path system for several reasons. First, in an open beam path system, the many optical components along the beam path from the laser to the engine cylinder must be kept precisely aligned in spite of significant vibration from the engine. Further, precise alignment must be maintained over long periods of time between servicing. On the other hand, optical fibers are inherently vibrationally robust. Using optical fibers allows the laser and multiplexer to be vibrationally isolated from the engine, significantly reducing potential misalignment. Second, safety is a concern in an open-beam path approach. Both infrared and visible light lasers are invisible as they propagate through space, thus it would be quite easy for an open-beam path laser beam to be interrupted accidentally by a reflective foreign object, redirecting away from its designated path and out into the open space around the engine. This situation poses a significant threat to the sight of people working on and around the engine. Safety is increased with optical fibers, since they totally contain the beam as it travels between the multiplexer and the engine, there is a considerably reduced risk that technicians working around the engine will accidentally encounter high-powered laser light.

However, this approach does have its own technical challenges to overcome. Multiplexing must be achieved while retaining consistent fiber alignment, and while transmitting laser powers sufficient for ignition. Researchers need to determine the optimum methods for multiplexing, for aiming the laser at multiple fibers at the right time, and for countering the problems associated with varied optical components placed along the high power beam path.

1.4 Problem Statement

The objective of this thesis research is to design, manufacture and test on the bench-top a practical multiplexer and spark-plug system to deliver one laser beam into two cylinders via hollow-core fiber optics, and to do so in a scalable manner that can later allow extension to any number of channels needed to ignite all the cylinders of an engine. In order to create a laser induced spark within the engine cylinders, the system must be able to focus laser light within the cylinder to an intensity of $\sim 1000 \text{ GW/cm}^2$ [7–10]. The system must also allow a sufficient delivered laser spark energy to ignite lean mixtures, of at least 10–20 mJ [2]. It must be able to operate for long time periods at the 120 Hz multiplexer switching and laser firing rate necessary to ignite one bank (8 cylinders) of a four-stroke Caterpillar G3516C engine running at 1800 rpm. And the system must maintain adequate alignment and energy delivery in spite of engine vibration and heat. To achieve these goals, constraints (Section 3.1) are placed upon the accuracy with which the laser is aimed at the fiber faces in the multiplexer, multiplexer switching speed, and laser spark timing.

2 Preliminary Development and Testing

2.1 Methods of Multiplexing

The methods used to investigate the multiplexing of one laser into multiple fibers can be broken roughly into two categories: solid-state and mechanical. The solid-state category may be further broken into *electro-optic modulators* (EOMs) and *acousto-optic modulator* (AOMs), and the mechanical category broken into *continuous rotation* and *step-and-hold* methods. Details about how these methods were chosen will be covered later in Section 3.3.

2.1.1 Solid-state Multiplexing Methods

Solid-state multiplexing allows for a very fast multiplexing system with no moving parts. Multiplexing via electro-optic and via acousto-optic modulators were considered for this project.

2.1.1.1 Electro-Optic Modulators

An electro-optic modulator consists of a non-linear optical crystal, whose optical properties are changed via the application of an electric field [35]. To accomplish the goal of multiplexing, electro-optic modulators which rotate beam polarization, such as Pockels cells, can be used along with polarizers and polarization-dependent mirrors, for example in a configuration shown in Figure 2.1 [36]. The system is polarization dependent, so the laser polarization should initially be prepared using a polarizer. The then light passes through an optical modulator, which when active, rotates the

polarization of the light by 90° , and when inactive, does not change the polarization of the light. The light then encounters a polarizing splitter, which allows the light to pass through unchanged for one polarized direction, and which reflects the light at a 90° angle for light polarized in the opposite, 90° rotated direction. This beam-splitter is arranged so that light will pass through it unreflected when the optical modulator just previous to it in the beam path is inactive. When the optical modulator is activated, the light will be reflected 90° and focused in to an optical fiber to be delivered to an engine cylinder. For each channel in the system, an optical modulator followed by a polarizing beam-splitter is used in series, with the last channel consisting of a single conventional 90° laser mirror (and being activated when all the optical modulators are off).

A typical Pockels cell has a transmittance of $> 98\%$ and a laser induced damaged threshold of $> 15 \text{ J/cm}^2$ for 10 ns duration pulses [37]. Assuming a maximum laser energy of 100 mJ, and an Nd:YAG laser with a beam diameter of 5 mm, and 8 ns pulse duration, and through the derivation shown in Section 4.2 and Equation 3.2, we find that the central spot intensity of the beam as it comes out of the laser has a maximum of 1.02 J/cm^2 , well below the damage threshold of our candidate electro-optic modulator. A typical high energy laser polarizing cube beamsplitter has a damage threshold of 5 J/cm^2 over 20 ns, which should be adequate for the laser intensity cited above [38]. It also has a transmission efficiency $T_p > 95\%$ for p-polarized light (vertically polarized in Figure 2.1), and a reflection efficiency $R_s > 99.5\%$ for s-polarized light (horizontally polarized in Figure 2.1). A typical high power Nd:YAG laser mirror has a reflectivity $> 99.5\%$ and a damage threshold of 20 J/cm^2 over 20 ns, which is adequate for this project's needs [39].

Given the above values for the transmittance and reflectance of components, an 8 channel multiplexer in the form of Figure 2.1 would have total transmittance values

for each channel as shown in Table 2.1, ranging from 98% for channel 1 to 59% for channel 8. Other configurations should have qualitatively similar performance.

Table 2.1: EOM Multiplexer Predicted Transmittance

Component	T_{total} (%)	$T_{channel}$ (%)	Channel #
OM	98.00		
BS	93.10	97.51	1
OM	91.24		
BS	86.68	90.78	2
OM	84.94		
BS	80.70	84.52	3
OM	79.08		
BS	75.13	78.69	4
OM	73.62		
BS	69.94	73.26	5
OM	68.54		
BS	65.12	68.20	6
OM	63.82		
BS	60.62	63.50	7
OM	59.41		
M	0.00	59.11	8

Calculated transmittance through an 8 channel electro-optic modulator-based multiplexer. T_{total} is the transmittance up to and through that component. $T_{channel}$ is the transmittance up to and reflected through the beamsplitter or mirror for each channel, this would be the percent of the laser output light reaching the channel's optical fiber. These results use the following component values: optical modulator transmittance, $T_{om} = 0.98$; beamsplitter transmittance, $T_{bs} = 0.95$; beamsplitter reflectance, $R_{bs} = 0.995$; laser mirror reflectance, $R_m = 0.995$ [37–39].

Pricing for electro-optic modulators was checked, and it was found that Pockels cells appropriate to the needs of this project have a typical price of about \$800 per unit. This works out to a cost of about \$11,200 for the electro-optic modulators for a multiplexer for a 16 cylinder engine consisting of two banks of 8 cylinders each [40]. Additionally, electro-optic modulator drivers would be needed to control and switch the Pockels cells, and mirrors and beamsplitters as needed.

2.1.1.2 Acousto-Optic Modulators

Acousto-optic modulators utilize the *acousto-optic* effect to diffract light along different paths. Instead of using electrical fields to change to optical properties of a crystal, they use piezo-electric transducers to induce acoustic waves in the material, causing the optical properties to change [41]. Acousto-optic modulators can be used in a similar way as electro-optic modulators in Figure 2.1. A typical acousto-optic modulator has a damage threshold of $> 1 \text{ GW/cm}^2$, which is more than sufficient for this application. It also has a transmittance of $> 99.6\%$, resulting in an updated Table 2.2 [42]. A challenge is that the light is generally diffracted into multiple orders (beams).

A typical price of \$2,500 per acousto-optic modulator was found, plus \$1,250 per driver unit. This results in a cost of \$26,250 for an 8 channel multiplexer based on acousto-optic modulators that would fit the needs of this project [43].

2.1.1.3 Summary of EOM & AOM Approaches

While solid-state methods of multiplexing are very fast, and allow for a great deal of adjustment along the beam-path from the laser to the fibers, they are relatively expensive due to the high cost of the optical modulators and the need for $n - 1$ modulators, where n is the number of fibers multiplexed into. This method of multiplexing also suffers from fairly high transmission losses due to the high number of optical components as well as the added complexity of compensating for the increasing transmission loss in each successive channel.

2.1.2 Mechanical Multiplexing Methods

A lower cost alternative to the solid-state optical modulators described above is that of mechanical multiplexing. This involves the use of a mirror which physically moves

Table 2.2: AOM Multiplexer Predicted Transmittance

Component	T_{total} (%)	$T_{channel}$ (%)	Channel #
OM	99.60		
BS	94.62	99.10	1
OM	94.24		
BS	89.53	93.77	2
OM	89.17		
BS	84.71	88.73	3
OM	84.37		
BS	80.16	83.95	4
OM	79.83		
BS	75.84	79.44	5
OM	75.54		
BS	71.76	75.16	6
OM	71.48		
BS	67.90	71.12	7
OM	67.63		
M	67.29	67.29	8

Calculated transmittance through an 8 channel acousto-optic modulator-based multiplexer. T_{total} in the transmittance up to and through that component. $T_{channel}$ is the transmittance up to and reflected through the beamsplitter or mirror for each channel, this would be the percent of the laser output light which makes it into each channel's optical fiber. These results use the following component values: optical modulator transmittance, $T_{om} = 0.996$; beamsplitter transmittance, $T_{bs} = 0.95$; beamsplitter reflectance, $R_{bs} = 0.995$; laser mirror reflectance, $R_m = 0.995$ [?, 38, 42].

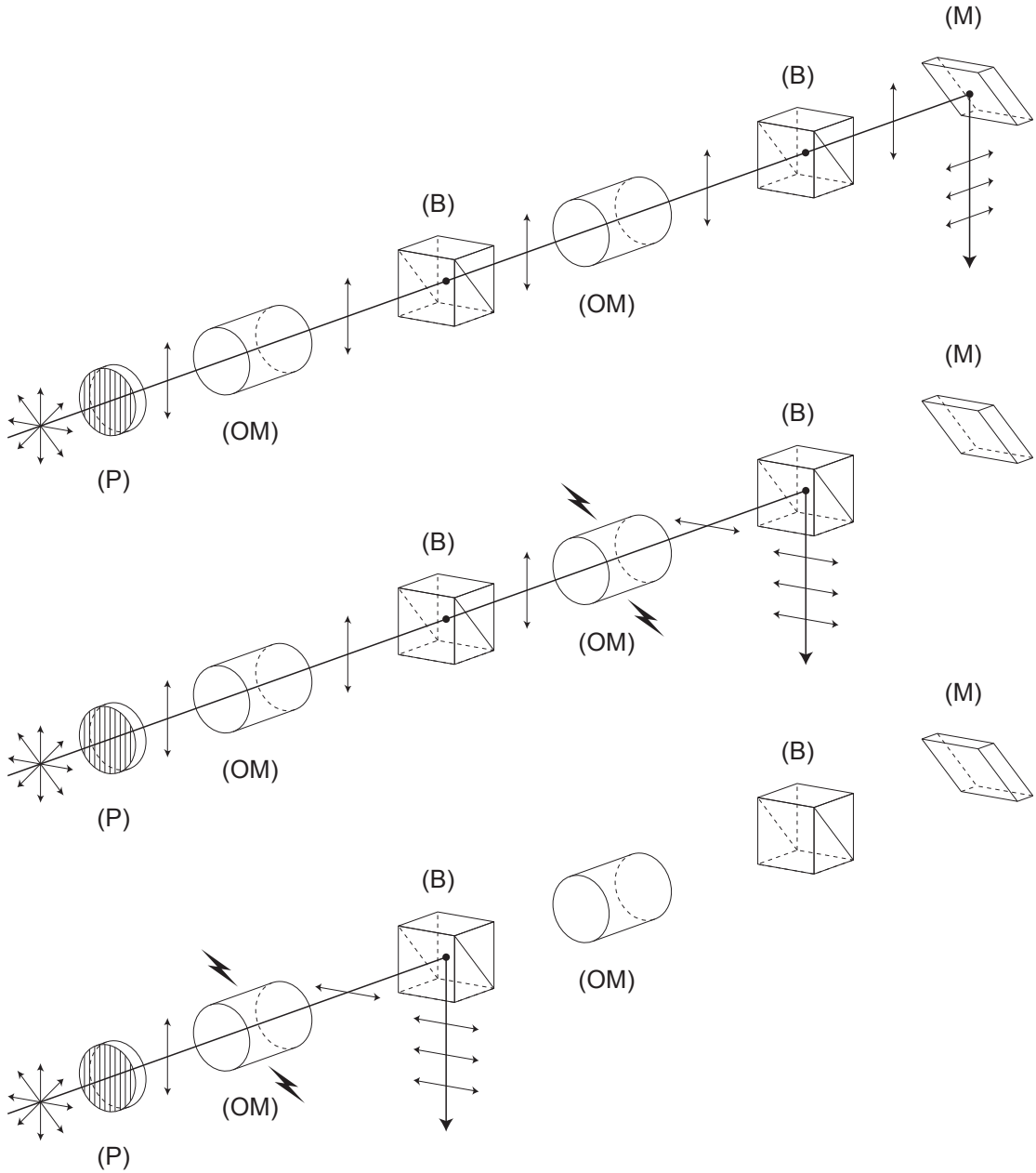


Figure 2.1: Schematic showing a three channel optical multiplexer employing polarization rotating optical modulators with no modulators active (top), the second modulator active (center, represented by lightning bolts), and the first modulator active (bottom), where (P) is a polarizer filter, (OM) are the optical modulators, (B) are polarizing splitter, and (M) is a normal laser mirror.

to direct incoming laser light into the desired output fiber.

Given representative launch parameters of $\theta_{launch} = 7 \text{ mrad}$, $w_{launch} = 254 \mu\text{m}$ and launch lens focal length of 50 cm covered in Section 1.2.1.1, a conservative estimate of needed launch precision for a 1 mm inner diameter hollow fiber of $\pm 100 \mu\text{m}$ was decided upon after experiments involving varying the alignment by hand. With the 50 cm focal length lens, this equates to a needed angular accuracy of 11.5 mrad for the multiplexing mirror, which would be just downstream of the launch lens. The needed speed and temporal accuracy are discussed in Section 3.1.

One method of mechanical multiplexing is the *continuous rotation method*. This involves, for example, affixing a mirror to the shaft of a motor at a 45° angle, such that light encountering the mirror coaxial with the motor is reflected out radially in an angular direction depending on the rotation of the motor. Fibers are then mounted radially in a circle around the mirror, such that with positional feedback from the motor, the laser may be fired at each fiber in sequence. Figure 2.2 shows a diagram of this method of continuous rotation multiplexing.

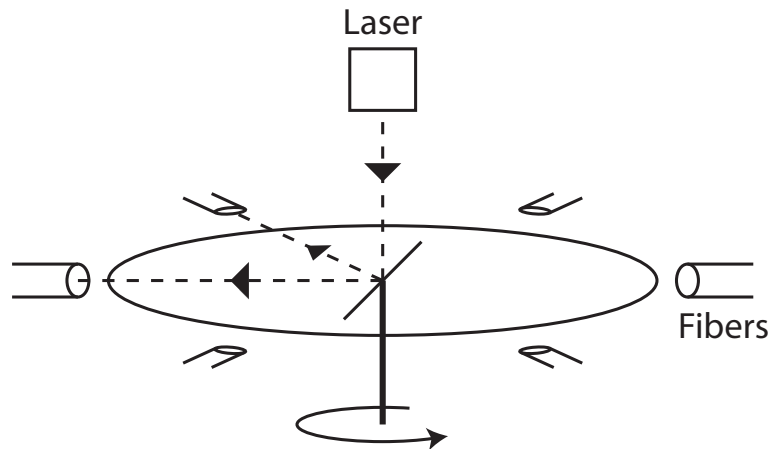


Figure 2.2: Schematic diagram showing a simple method of multiplexing via the continuous rotation method.

The continuous rotation approach allows for relatively simple design, and may

give the lowest cost for physical components. On the other hand, this approach does not readily permit timing adjustments on individual channels, and with constant revolution speed can only advance or retard the timing of all channels relative to engine cylinders as a whole. Additionally, very precise and accurate positional feedback from the motor is required to aim the laser into each fiber, and the software to control the system would be complex.

The second method for mechanical multiplexing is that of the step-and-hold approach. In this method, a mirror is pointed at the appropriate fiber and held there, the laser is fired, then the mirror is pointed at the next position. A schematic view of this method of multiplexing is shown in Figure 2.3. One way of pointing a switching mirror in this way is through the use of a high precision piezoelectric stack(s) affixed to a mirror such that the expansion and contraction of one (or two) stack(s) cause the mirror to rotate along one or two axes, respectively. While piezoelectric stacks do provide very high precision, they do not have a range large enough for ready implementation into the intended design [44]. An alternate way to switch the mirror in the step-and-hold approach is to use a galvanometer, which is a magnetic coil-based device that can rotate an attached mirror to any position within its range of sweep. Galvanometers can be used singly for single axis beam pointing, or in a pair to provide dual axis pointing. While more expensive than the motor described for continuous rotation multiplexing, they are still relatively low cost and are commercially available for laser scanning applications.

Pricing for a galvanometer (Cambridge Technology 6210H) with 6mm X mounted (long axis of the mirror mounted perpendicular to the turning axis, to allow for the elongation of a laser spot directed at the mirror at an angle of $\approx 45^\circ$) YA coated (high power Nd:YAG 1064 nm high reflectivity coating) mirror with analog controller board was quoted as \$1,320 [45]. This is significantly lower cost versus solid-state

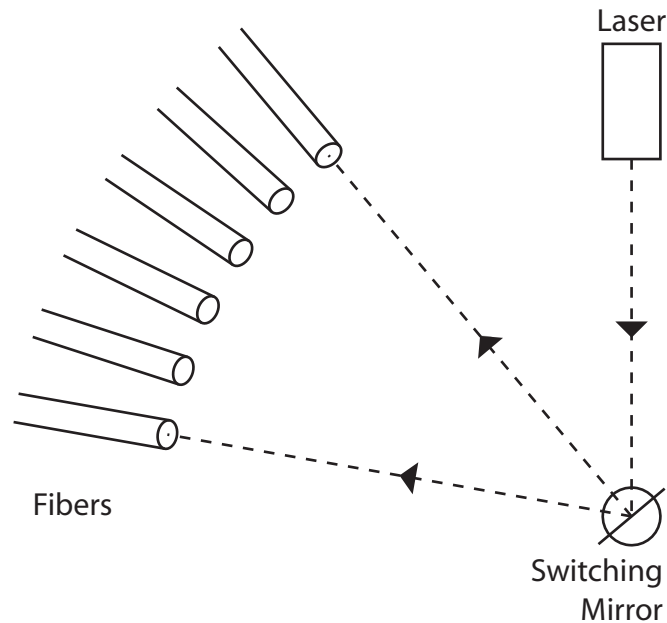


Figure 2.3: Schematic diagram showing multiplexing via the step-and-hold method.

multiplexer components.

2.2 Initial Galvanometer Test

A galvanometer (Cambridge Technology, 6210H) with 6mm Nd:YAG mirror was chosen for the initial proof-of-concept mechanical multiplexer tests. A step-and-hold approach with a galvanometer was chosen for its low cost, ease of use, and quick setup time; the galvanometer connects to an included controller board, which is controlled with a -10 V to $+10\text{ V}$ external signal. The control signal was generated by a LabView program, and was output through a digital to analog converter PC card.

First, a speed test was conducted wherein a stepped control signal, representing a 6 cylinder engine running at 1800 rpm, was sent to the galvanometer. Figure 2.4 shows an example of two cycles of the stepped control signal. A 543.5 nm green continuous-wave (CW) helium-neon laser was aimed at the galvanometer and a paper target positioned to intercept the reflected light. The pattern of 6 dots on the paper target

is shown in Figure 2.5. This test was considered a success because the galvanometer had no trouble keeping up with the control signal, and there was only a very faint trace of light visible between the dots and the paper target, demonstrating that the galvanometer was moving between positions very quickly.

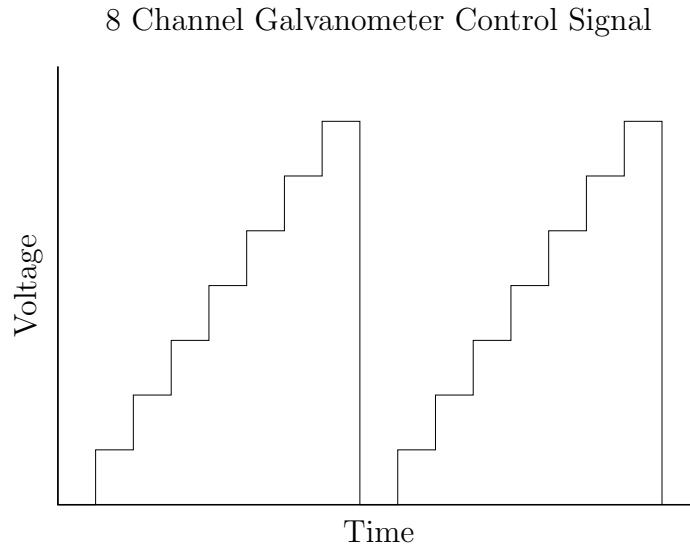


Figure 2.4: Plot of two cycles of the galvanometer control signal with eight channels. After channel 8, the signal drops back to channel 1.

The second galvanometer test involved generating sparks through two separate fibers. For this test, a simple square wave was fed to the galvanometer to cause it to switch between the two positions corresponding to the two fibers. A 50 cm focal length launch lens was placed in the beam path about 2 cm upstream of the galvanometer mirror. Final focusing optics, consisting of a 35 mm focal length lens followed by a 12 mm focal length lens, were placed about 10 cm from the fiber ends. Figure 2.6 shows a schematic setup of the arrangement, where the laser beam goes through a launch lens and is deflected by the galvanometer into one of the two fibers, at the end of which are positioned focusing optics. A LabView program was written to control and synchronize the galvanometer and firing of the laser. Using this setup, sparking was reliably achieved through both optical fibers at a rate equivalent to two opposite

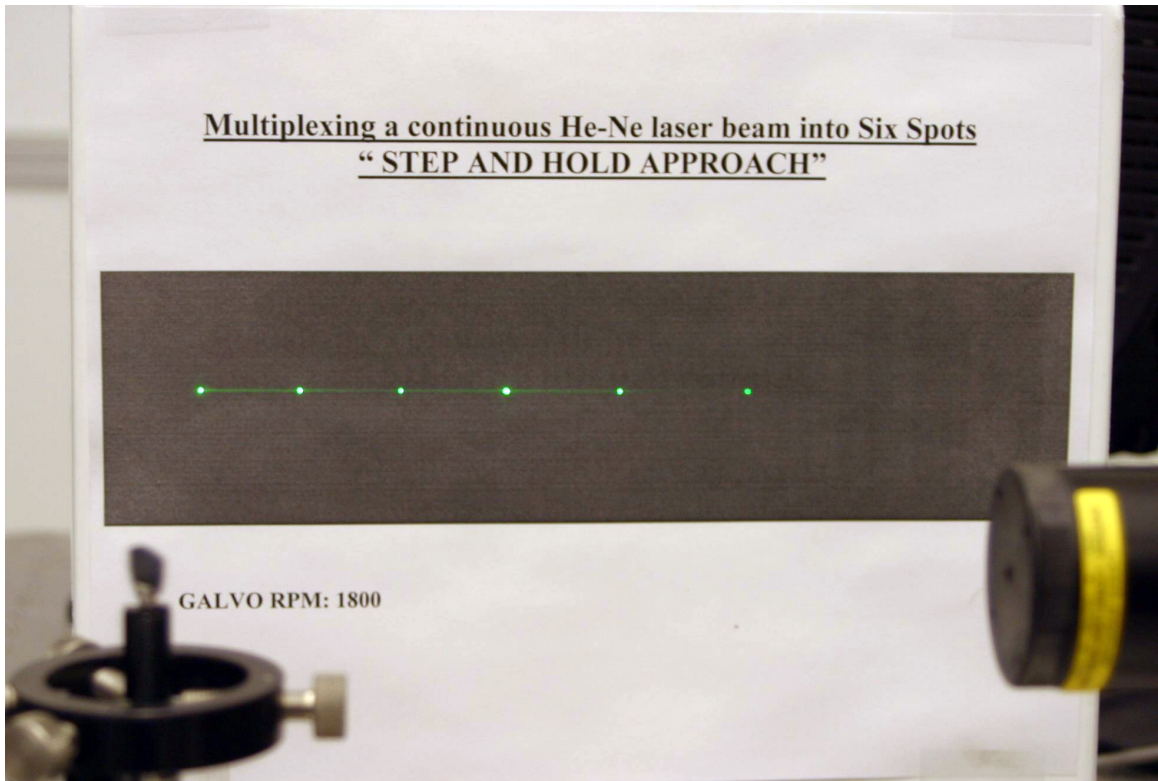


Figure 2.5: Photograph showing the initial galvanometer test at the equivalent speed of a six cylinder, four-stroke engine running at 1800 rpm. The helium-neon laser is at the bottom right, the galvanometer is at the bottom left, with the series of reflected dots above, showing the laser multiplexed into six channels. The dots increase in distance from left to right due to the orientation of the paper target with respect to the galvanometer, where the left side is closer than the right.

phase cylinders in a four-stroke engine running at 1800 rpm.

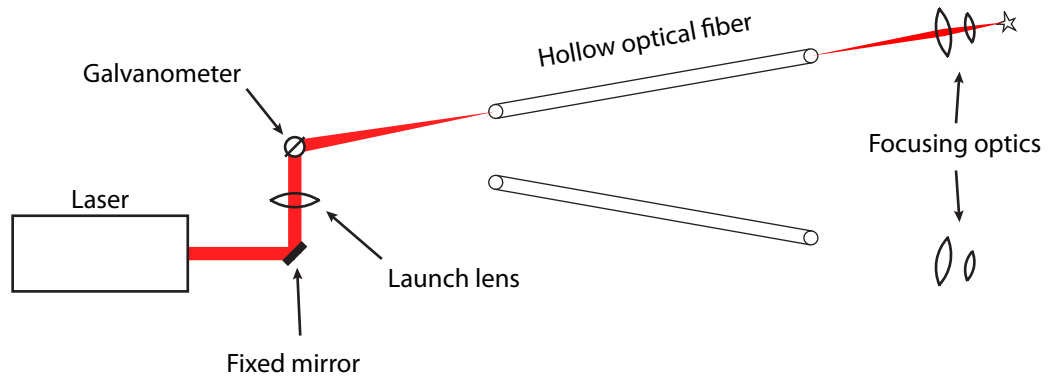


Figure 2.6: Schematic setup of the galvanometer spark test. The laser beam passes through the launch lens before encountering the galvanometer, which directs the beam into one of two hollow optical fibers. When the beam exits the fiber, it goes through two focusing lenses, which focus it to a point at which a spark is formed.

3 Multiplexer Design

3.1 Design Constraints

Practical multiplexer designs must meet basic design constraints of the engine ignition system. These include switching speed, determined by the speed of the chosen engine, and fiber launch accuracy, which is how close to the center axis the laser must be aimed into the fiber.

The engine for which this multiplexer was designed is a 4-stroke Caterpillar G3516C with a nominal running speed of 1800 rpm. The engine has two banks of 8 cylinders, with a configuration as shown in Figure 3.1, where each bank completes a full engine cycle independently, with the two cylinder banks interleaved. Due to the limitations of bending hollow fibers, the multiplexer was designed to operate at a maximum of 8 cylinders in a single bank of the engine. For a 4-stroke engine at 1800 rpm, each cylinder in the 8 cylinder bank fires every 66.67 ms, with a time between consecutive cylinder firings of 8.33 ms. This means that the multiplexer must be able to switch between fibers at a rate of 120 Hz for one bank of the engine.

The hollow fibers used throughout the tests have an inside diameter of 1000 μm . Alignment was generally accomplished by hand, using a yellow sticky note held up to the fiber face, which fluoresced to show the beam position. The aim of the laser was adjusted accordingly, using a conservative estimate of $\pm 100 \mu\text{m}$ for the launch accuracy. It is the repeatability of the fiber launch within this accuracy which is important, since the beam is initially aligned by hand to optimize laser throughput.

The multiplexer must function next to a running engine for indefinite periods of

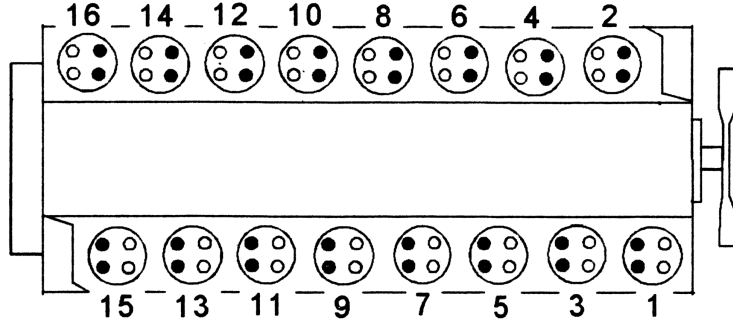


Figure 3.1: Top-view of the engine cylinder configuration in a Caterpillar G3516C engine. The cylinders on each bank of the engine complete a full cycle, with each bank interleaved with the other.

time, so all optical and mechanical components must be able to maintain this accuracy in spite of engine vibration and heat, and the optical or mechanical switches within the multiplexer must be able to sustain this switching speed indefinitely.

3.2 Simulations

Due to the high energy of the beam, careful design was necessary to ensure that the light intensity on the various optical elements in the beam path did not exceed their respective *laser induced damage thresholds* (LIDTs). In order to ensure that the laser beam doesn't damage any parts within the multiplexer, the beam's size and central maximum intensity were modeled from the laser, through the launch lens to the focal point at the fiber faces. First, the beam's central maximum intensity was calculated as it comes out of the laser, before any optics. The irradiance intensity distribution for a Gaussian beam is:

$$I(r) = I_0 e^{-2\frac{r^2}{w^2}} = \frac{2P}{\pi w^2} e^{-2\frac{r^2}{w^2}} \quad (3.1)$$

where P is the total power in the beam, w is the beam spot size radius, and r is the radial distance from the beam axis [46]. Note that the beam exiting the laser is nearly single-mode ($M^2 \approx 1$), so that use of the Gaussian expression is appropriate .

For short pulses, the total energy in the pulse is more often used instead of power, in which case the central beam fluence can be determined as:

$$F_{center} = \frac{2E}{\pi w^2} \quad (3.2)$$

where E is the beam energy. Given a maximum laser energy of 100 mJ in 8 ns, and a beam diameter of 5 mm, a central beam fluence of 1.02 mJ/cm² was found for the beam as it exits the laser.

Next, the central beam fluence was modeled along the beam from the 50 cm launch lens to the fiber faces. The complex beam parameter is given by [47]:

$$\frac{1}{q(z)} = \frac{1}{R(z)} - i \frac{\lambda_0}{\pi n w(z)^2} \quad (3.3)$$

where $q(z)$ is the complex beam parameter at the point z along the beam, $R(z)$ is the radius of curvature of the phase front at z , λ_0 is the laser wavelength, and $w(z)$ is the beam waist at z . The $ABCD$ ray matrix for a thin lens followed by a distance of free space z is [47]:

$$T = \begin{bmatrix} A & B \\ C & D \end{bmatrix} = \begin{bmatrix} 1 - \frac{z}{f} & z \\ -\frac{1}{f} & 1 \end{bmatrix} \quad (3.4)$$

where f is the lens's focal length and z is the distance from the lens. Given an optical component defined by an $ABCD$ ray matrix, the transformed complex beam parameter q' is defined as [47]:

$$q' = \frac{Aq + B}{Cq + D} \quad (3.5)$$

The reciprocal of which is more relatable to Equation 3.3:

$$\frac{1}{q'} = \frac{C + D \frac{1}{q}}{A + B \frac{1}{q}} \quad (3.6)$$

If we assume that the wavefront impinging upon the lens is planar (which can be achieved with a collimated beam), substituting the matrix elements from Equation 3.4 into Equation 3.6 and separating the real and imaginary parts yields the following equation for the complex beam parameter as a function of the distance z after the lens:

$$\frac{1}{q(z)} = \frac{-\frac{1}{f} + z \left(\frac{1}{f^2} + \frac{1}{z_0^2} \right)}{\left(1 - \frac{z}{f} \right)^2 + \left(\frac{z}{z_0} \right)^2} - i \frac{\frac{1}{z_0}}{\left(1 - \frac{z}{f} \right)^2 + \left(\frac{z}{z_0} \right)^2} \quad (3.7)$$

where $z_0 = \frac{\pi w_0^2}{\lambda_0}$, f is the lens's focal length, λ_0 is the laser wavelength, and w_0 is the beam radius before hitting the lens. Comparing Equation 3.7 to Equation 3.3 we see that:

$$\frac{\lambda_0}{\pi w(z)^2} = \frac{\frac{1}{z_0}}{\left(1 - \frac{z}{f} \right)^2 + \left(\frac{z}{z_0} \right)^2} \quad (3.8)$$

Solving for $w(z)^2$ gives:

$$w(z)^2 = w_0^2 \left[\left(1 - \frac{z}{f} \right)^2 + \left(\frac{z}{z_0} \right)^2 \right] \quad (3.9)$$

Given equations 3.2 and 3.9, Figure 3.2 shows the modeled central intensity of the beam from the launch lens to the focus, 50 cm downstream, given a pulse energy of 100 mJ. A typical high power Nd:YAG laser mirror has a damage threshold of 20 J/cm² over 20 ns [39], and as can be seen from the figure, the central beam energy does not rise to this level until about $z = 38$ cm. Any multiplexer design must take into account the intensities shown in Figure 3.2 when introducing any optics after the launch lens, particularly when approaching within 12 cm of the beam focus.

3.3 Design Overview

As discussed in Section 2.1, a mechanical method of multiplexing one laser into multiple fibers was chosen due to the much lower cost of this approach versus the

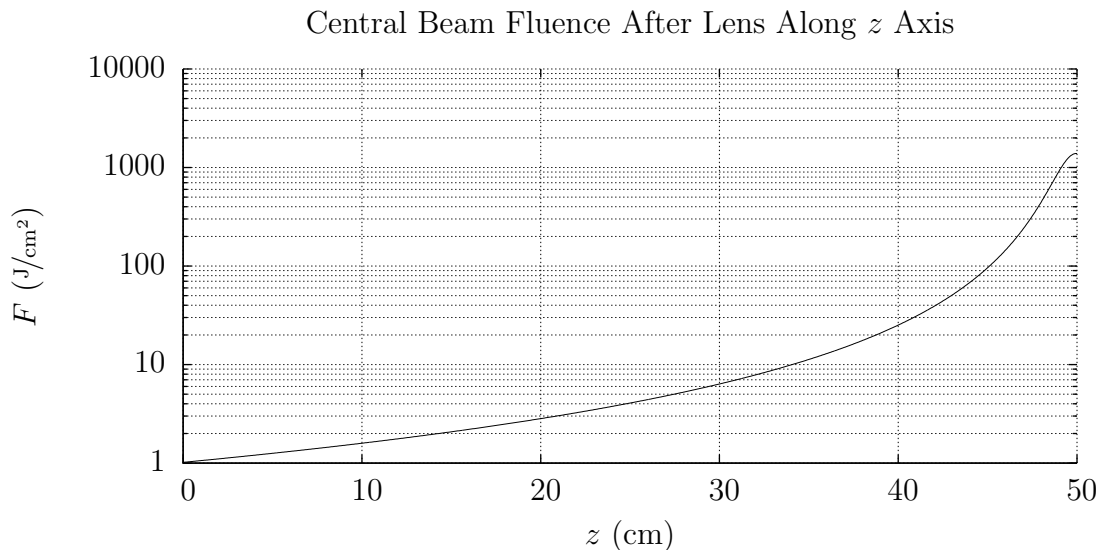


Figure 3.2: Central fluence of the beam from the launch lens until the focus 50 cm later, given a pulse energy of 100 mJ.

others presented. In discussions with Woodward Industrial Controls—one of the project sponsors who machined the parts for the multiplexer and were involved in the design—it was decided that a continuous rotation approach employing a prism with a parallelogram cross-section for the multiplexer would first be examined due to the perceived robustness of the design. In this approach, a prism is mounted on the axle of a motor such that its entrance face is on the axis, while the exit face is offset from the axis, thus tracing a circle determined by the rotation of the motor as in Figure 3.3. A vacuum is needed to launch the laser beam into the fibers without sparking in the air at the focal point and fiber faces, and a port was used to make a vacuum connection. The laser beam enters coaxial with the motor shaft, first going through a 2.54 cm diameter, 50 cm focal length, launch lens, which also acts as a window into the vacuum chamber which contains the motor, prism, and fiber faces. The total launch tube length from launch lens to fiber faces was 40 cm to accommodate the 10 cm offset that the prism would introduce. The beam then enters the prism and is reflected such that the beam exits parallel to the axis but offset by 10 cm. Thus

the focal point of the beam traces a circle with a radius of 10 cm, and it is along this circle that the multiple fibers are mounted. Figure 3.4 shows an exploded view of the various multiplexer parts, where the beam enters the vacuum chamber through the launch lens, then goes through the rotating prism assembly mounted to the motor, is directed through the vacuum chamber launch tube, and finally into the fibers mounted in the fiber holder. Figure 3.5 shows the multiplexer assembled, with the launch lens, vacuum chamber parts, and the fiber holder with fibers exiting the rear. Appendix A-1 contains technical drawings of the multiplexer parts.

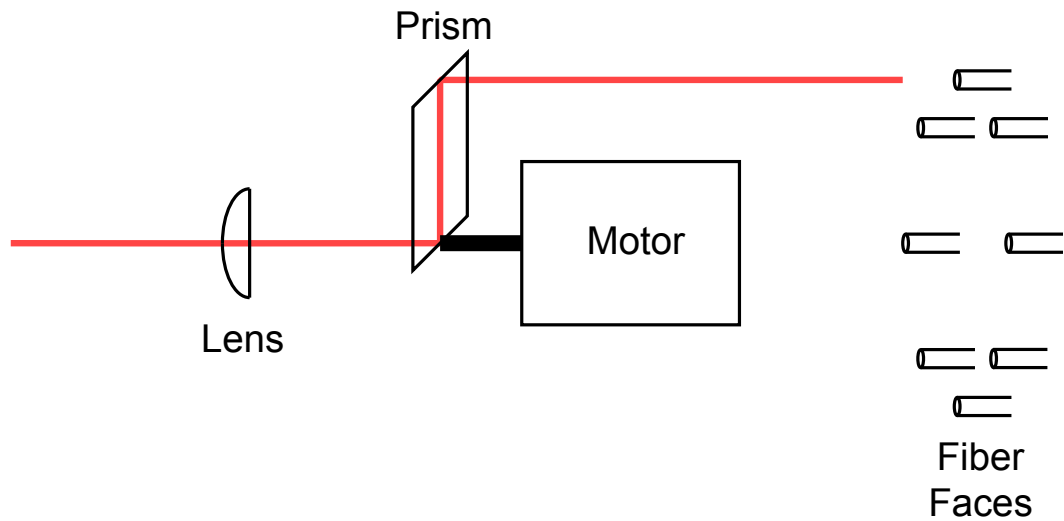


Figure 3.3: Schematic diagram of mechanical multiplexer employing a continuously rotating prism. The beam is shown coming from the left, passing through the launch lens, then being diverted by the prism and entering one of the eight fibers.

Through discussions with Woodward, aluminum was chosen for the multiplexer parts due to its lightness and ease of machining as compared to steel, as well as its rigidity and durability as compared to plastics.

Originally, it was decided that Woodward would provide the control software for

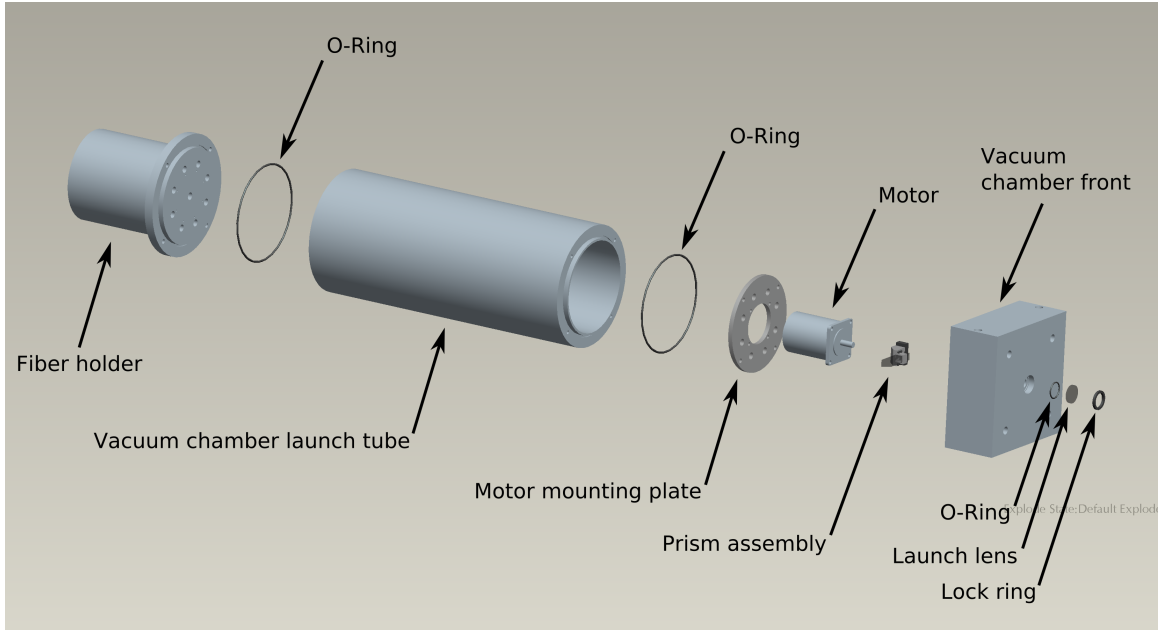


Figure 3.4: Exploded view of the multiplexer showing the placement of the motor and prism assembly.

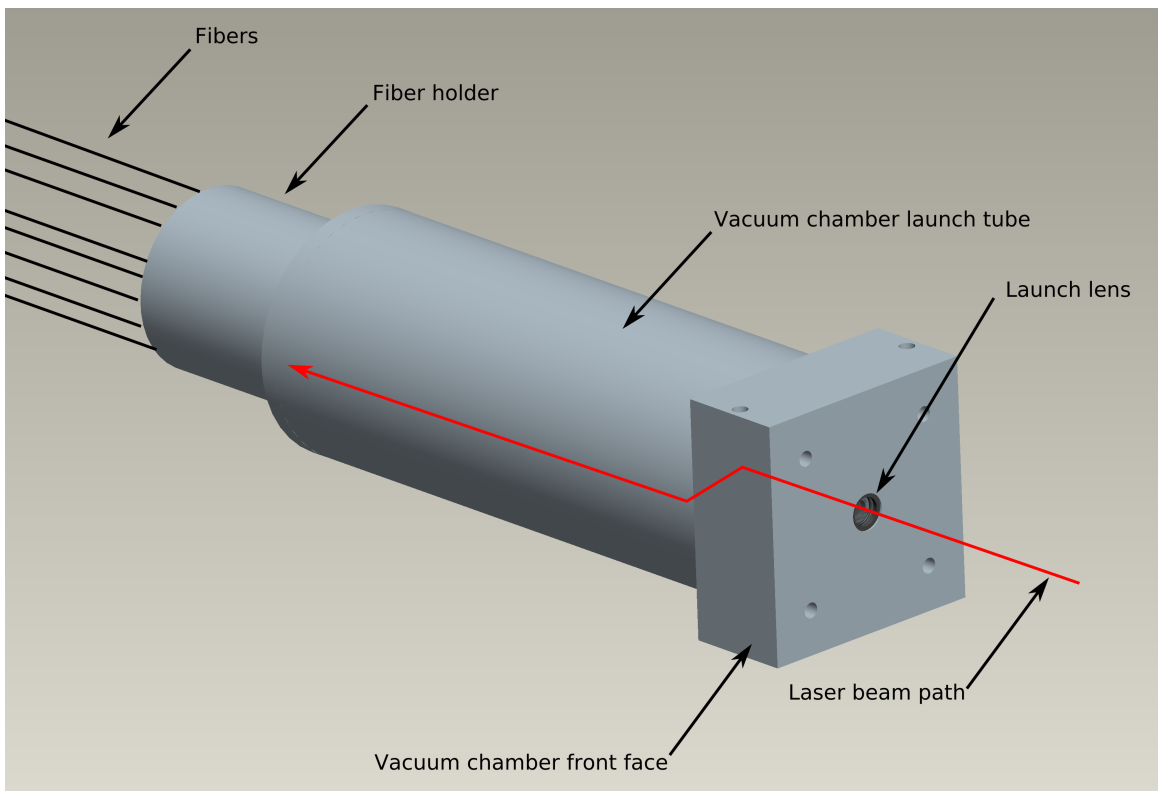


Figure 3.5: Assembled view of the multiplexer showing the path which the laser beam takes for one of the fibers.

the multiplexer motor. But due to a series of delays, a new plan for motor control was devised by which a mirror was mounted on a step-and-hold galvanometer to direct the beam, instead of using a prism mounted on a continuously rotating motor. As discussed in Section 2.2, a galvanometer had originally been tested for speed and the ability to spark with two fibers.

To accommodate the galvanometer, the launch lens was replaced with a sapphire window, which was chosen for its durability and high laser intensity damage threshold, with the galvanometer mounted a few centimeters before the window, and the launch lens mounted just before the galvanometer in the beam path, as shown schematically in Figure 2.3 and shown as a 3D drawing in Figure 3.6. The window needed to be mounted back along the beam path by about 10 cm because there was no longer a 10 cm detour being introduced by the prism inside the launch tube. A slot in the mounting plate was machined so that the lens could be adjusted forward and backward to adjust the focus of the beam at the fiber faces (and was rotated slightly off-axis to keep back-reflections from entering the laser). Due to the single pointing axis given by the galvanometer, this retrofit setup allowed the laser to be launched into one of two fibers, instead of the one of eight in the previous setup. This did not present a problem as initial engine tests involved only two cylinders. The fiber holder block did need to be re-machined with new fiber mounting holes angled inward toward the galvanometer mirror instead of the original design which featured parallel holes.

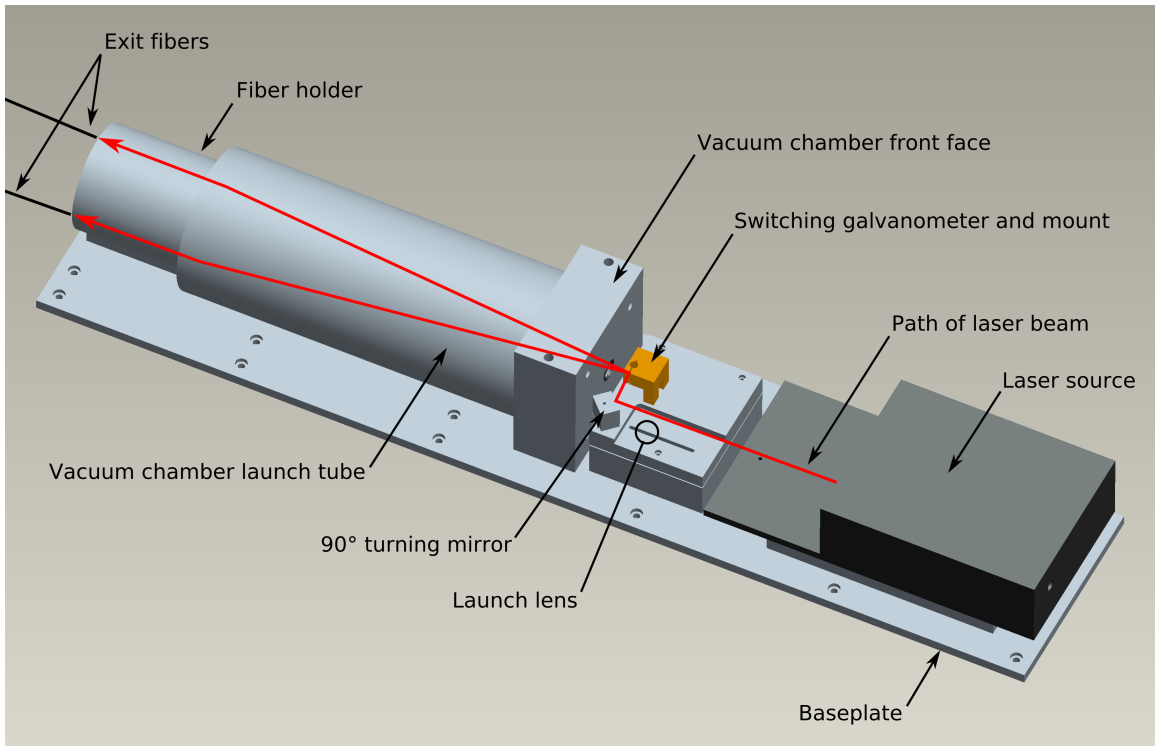


Figure 3.6: Assembled view of the modified multiplexer showing the galvanometer placement and beam paths for the two fiber channels.

4 Spark Plug Design

4.1 Introduction

As a final step, in order to focus the laser light exiting the multiplexed fiber optics, an optical spark plug for the Caterpillar G3516C engine is needed. The optical sparkplug screws into the existing spark plug socket, and includes a window and focusing optics. The final focused beam provides the igniting sparks in the engine cylinder. Due to the limited bending ability of the hollow fibers, the spark plug also includes a 90° turning mirror such that the fibers can enter the spark plug parallel with the ground, thus minimizing the bending required of the fibers between the multiplexer and the sparkplugs.

4.2 Design Overview

Figure 4.1 shows a schematic view of the sparkplug design. The laser light exits the fiber, encounters the 5.08 cm 90° turning mirror, goes through a 2.54 cm collimation lens, down the barrel, and finally through the focusing optics and window. Since the intensity at the 90° turning mirror needed to be lower than its *laser induced damage threshold* (LIDT), exact calculations of the distance between the fiber exit and the mirror were deemed important. Given that the beam size at the fiber exit is 0.5 mm, the M^2 of the beam is at least 15, the 90° mirror, sourced from *CVI Laser*, has an LIDT of 20 J/cm^2 , and the laser pulse energy of 50 mJ, the minimum distance from the fiber exit face to the 90° turning mirror can be found as follows:

The spot size of a Gaussian beam in air z units along the axis from the waist is:

$$w(z) = w_0 \left[1 + \left(\frac{z\lambda M^2}{\pi w_0^2} \right)^2 \right]^{1/2} \quad (4.1)$$

where $w(z)$ is the spot size radius at z , w_0 is the waist size radius, λ is the wavelength, and M^2 is the propagation constant as described earlier [46–48]. Equation 4.1 does not account for unpredictable hot spots (spikes) in the non-Gaussian multi-mode beam (where $M^2 > 1$) exiting the fiber. We can account for this by allowing for at least a factor of 2 safety margin when determining the energies impinging on optical components. Solving Equation 4.1 for z gives:

$$z = \frac{\pi w_0^2}{\lambda M^2} \left[\left(\frac{w(z)}{w_0} \right)^2 - 1 \right]^{1/2} \quad (4.2)$$

The next calculation determined the minimum spot size at which the beam could hit the mirror without exceeding the LIDT. As shown in Section 3.2, the central energy fluence (J/cm^2) is:

$$F_{center} = \frac{2E}{\pi w^2} \quad (3.2)$$

where E is the beam energy and w is the spot size. Solving Equation 3.2 for spot size, and given that the fluence scales as $\cos(\theta)$ of the mirror, yields:

$$w = \left[\frac{2E}{\pi F_{center} \cos(45^\circ)} \right]^{1/2} \quad (4.3)$$

Given $E = 0.050 \text{ J}$, and $F_{center} = LIDT_{mirror} = 20 \text{ J}/\text{cm}^2$, $w = 0.47 \text{ mm}$. This is actually less than the fiber exit radius (and beam waist at the fiber exit), so it was decided that any distance from the mirror was acceptable.

Figure 4.2 shows an exploded view of the sparkplug design, while Figure 4.3 shows an assembled view. As shown in the figures, the sparkplug consists of three major

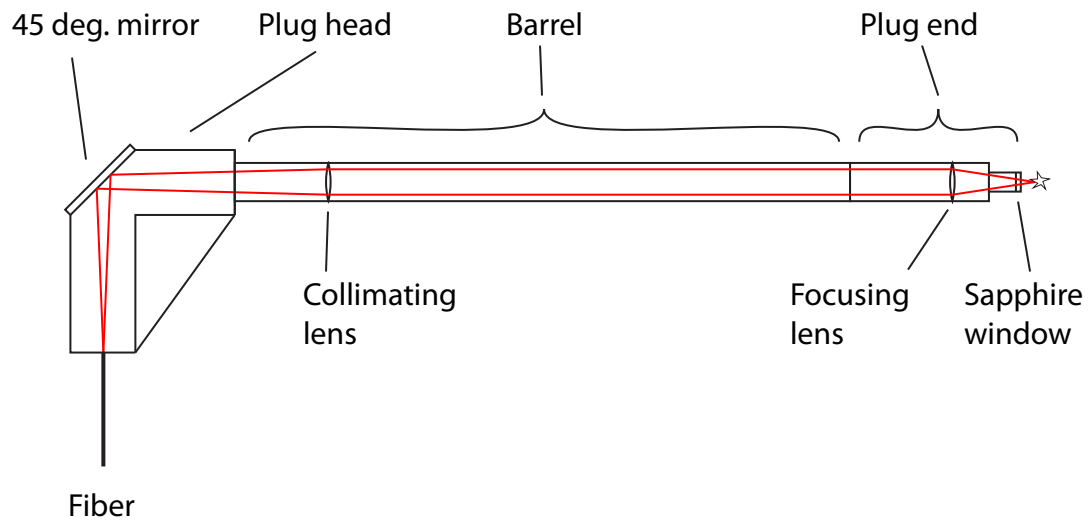


Figure 4.1: Schematic view of the spark plug design, where the laser beam exits the fiber, makes a 90 degree turn on the 45 degree mirror, is collimated with the collimating lens, goes down the barrel and is focused with the final focusing lens through the sapphire window to a point, where a plasma spark is formed inside the engine cylinder. While the diagram is shown horizontally, the spark plug is mounted vertically on the engine, with the fiber coming in horizontally and the barrel pointing down into the engine cylinder from above.

segments: the head, barrel, and end section. The head contains a fiber chuck insert which can be adjusted backward and forward coaxial with the beam to allow the distance from the fiber exit face to the turning mirror to be fine tuned depending on the M^2 of the exit beam. This chuck is fixed in place by set screws which come in from the top and sides of the head. Also mounted to the head is the 90° turning mirror, which is pressed into place on top of an o-ring with a compression plate and four screws. The barrel screws into the sparkplug head and lifts it up above the engine casing and valve components on the cylinder head. The relatively long length of the barrel is due to the design of the engine and ideally it could be made more compact from an optical view. The collimating lens is mounted within a lens carriage (Figure 4.4) which is threaded into the top portion of the barrel. This carriage allows the lens to be positioned to best optimize the beam size at the end section. The end section threads onto the barrel, and is internally threaded to accept the following: a sapphire window, the final focusing lens carriage, and the first focusing lens with spacers and compression ring. Figure 4.5 shows the end section in more detail. Appendix A-2 contains technical drawings for some of the sparkplug parts.

Vacuum is maintained in the spark plug through a pump connected to the plastic tubing used to sheath the hollow fibers. The spark plug utilizes the following components to preserve the vacuum within: Swagelok fittings to interface the plastic tubing carrying the fiber to the head; o-rings under the turning mirror and around the top of the barrel; and copper washers between the barrel and end section, as well as sandwiching the sapphire mirror. Copper washers, instead of rubber o-rings, were used at the end sections of the plug for heat-resistance.

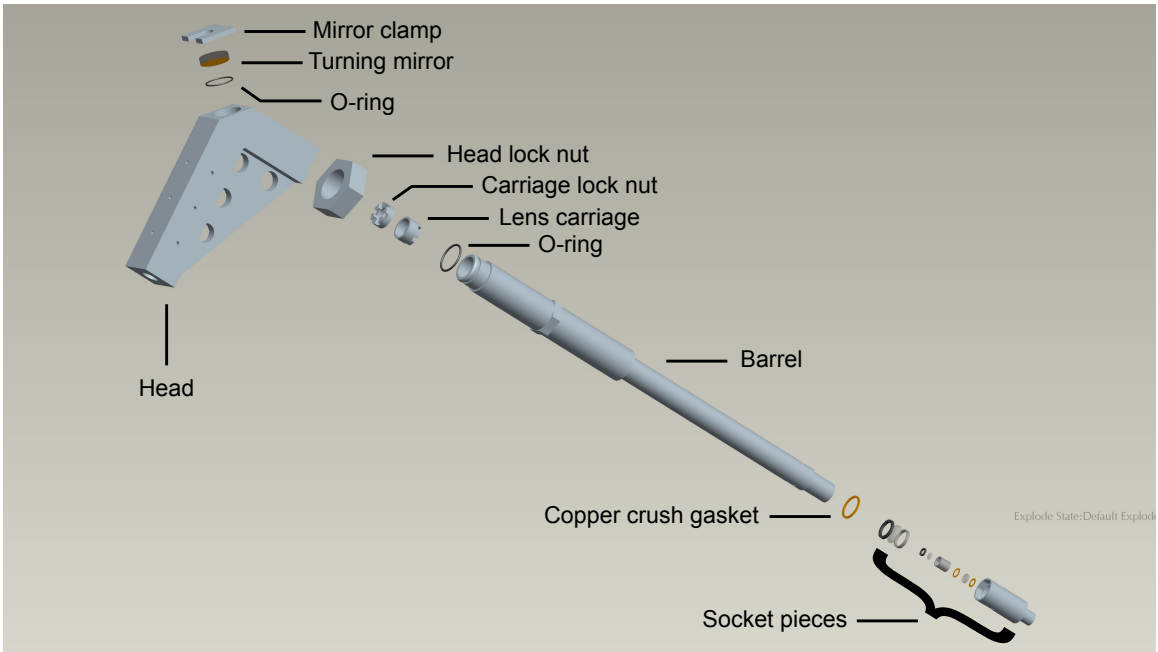


Figure 4.2: Exploded view of the sparkplug design.

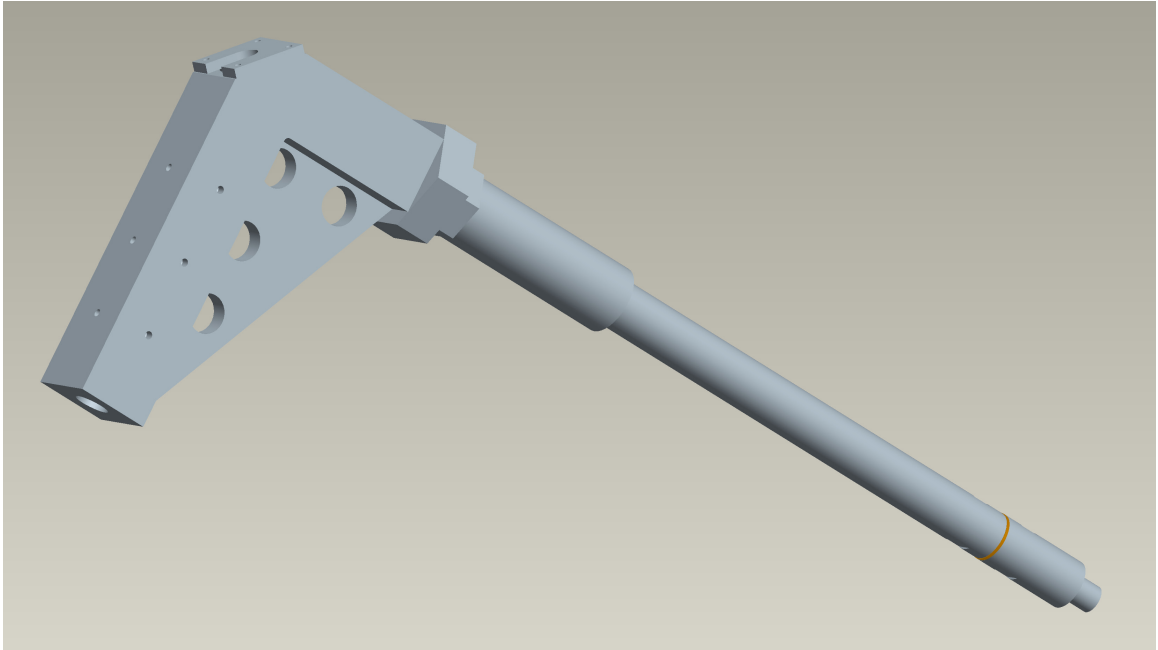


Figure 4.3: Assembled view of the sparkplug design.

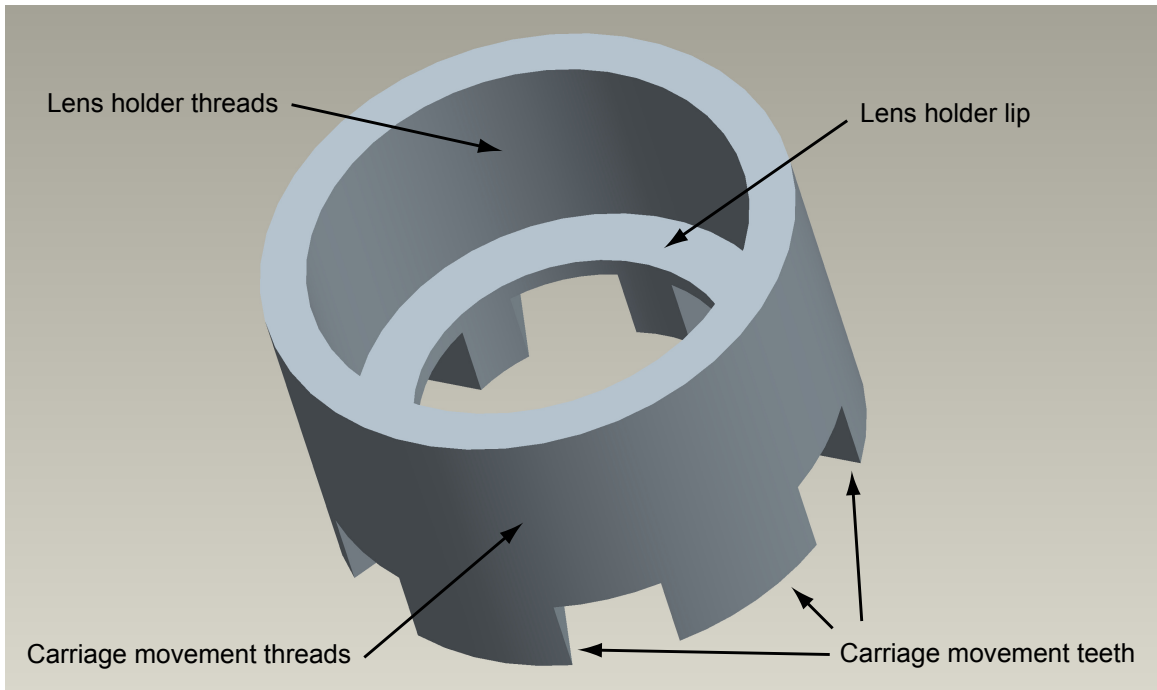


Figure 4.4: Lens carriage design.

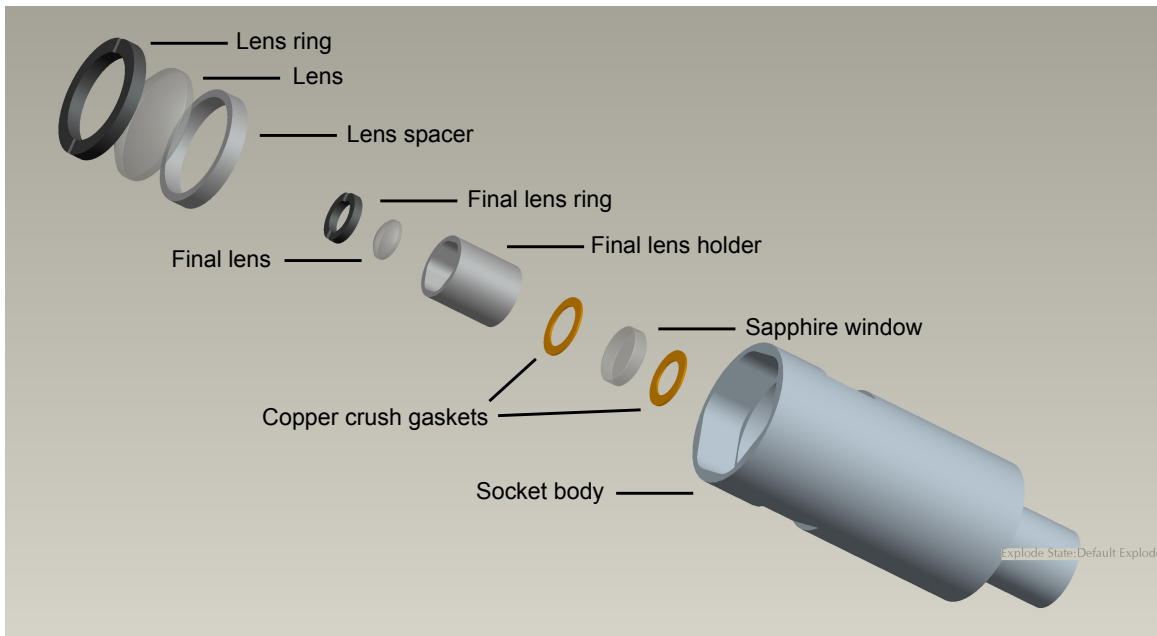


Figure 4.5: Exploded view of the sparkplug end socket. The assembled socket shows only the socket body.

4.3 Post Design-Phase Changes

Some changes to the sparkplug needed to be made in the post-design and initial testing phases.

First, Woodward discovered while machining the sparkplug barrel that the barrel was too long to cut the internal threads, so it was split into two pieces at the interface between the top and bottom portions of the barrel. The final two pieces of the barrel screw together and hold vacuum with the use of some Teflon tape.

Next, it was found that due to imperfect alignment, a limited amount of directional pointing was needed for the 90° turning mirror in order for the beam to be centered at the end section. This required the design of a new mirror compression clamp shown in Figure 4.6. This replacement clamp uses three screws and has a lip, which in concert with a thicker o-ring, allows the mirror a few degrees of angular adjustment while retaining a vacuum seal. The head section had to have three new screw holes drilled to accept this new mirror clamp.

Further, a plug had to be made to fit into the head to interface the fiber tubing with the head. The plug fits the front face of the head and is made to accept a Swagelok fitting to mate with the tubing. The plug must be removed and reinserted every time the fiber is removed or inserted due to the insert and fiber chuck being too big to fit through the plug.

Additionally, during initial testing of the sparkplug and multiplexer (as discussed later in Section 5), it was determined that the axial fiber location adjustment built into the head design was unnecessary, so the fibers were fixed near their outermost position.

Finally, initial testing also revealed that the first focusing lens in the end section was unnecessary (consistent sparking was attainable without it), and throughout testing only the final focusing lens in concert with the collimating lens was used.

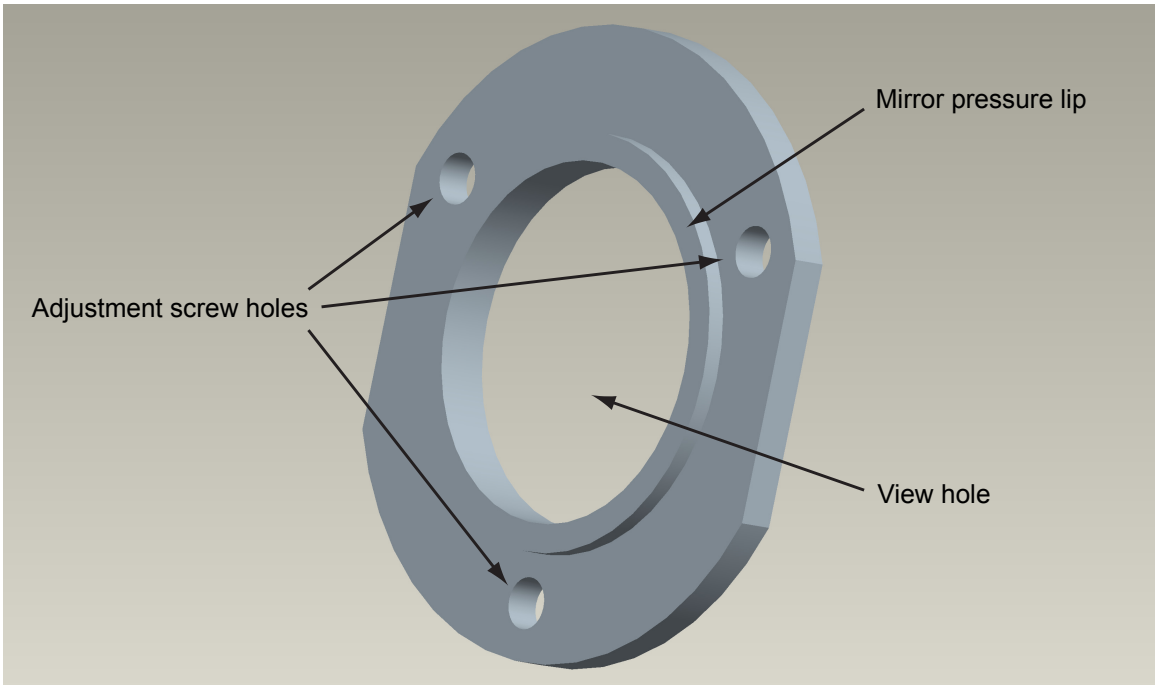
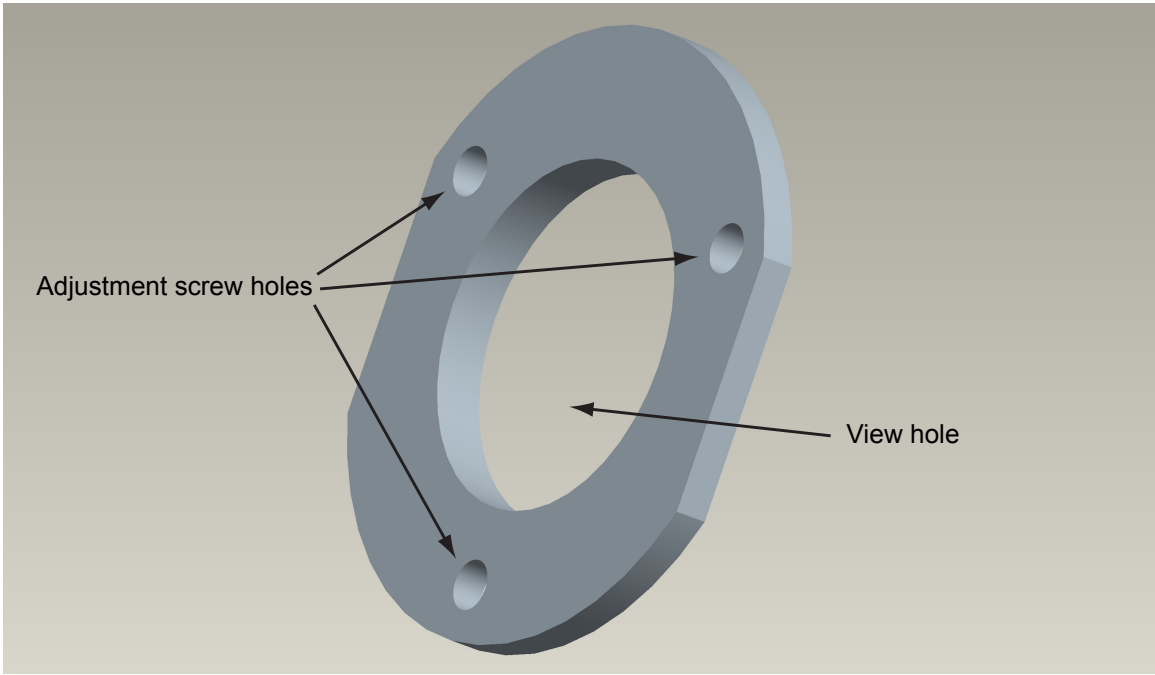


Figure 4.6: Front and back view of redesigned mirror clamp.

5 Multiplexer Tests

5.1 Bench-top Tests

Bench-top tests of the entire assembled multiplexing system were performed in order to identify and resolve problems before on-engine tests.

5.1.1 Setup

For preliminary bench-top multiplexer testing, the laser and multiplexer were attached to their common base-plate, with two fibers exiting the end of the multiplexer and, with minimal bending, entering the two spark-plugs. The fibers were sheathed in nylon tubing such that the vacuum could be carried from the multiplexer to the spark-plugs. For bench-top testing, the spark-plugs were placed in a horizontal orientation, versus the slightly off-from-vertical orientation to be used on-engine.

It was possible to disconnect the assembly at a number of points along the beam path in order to gain access to the beam to measure energy and beam profile. The points at which data were measured are as follows: just after the laser; just after the galvanometer mirror; before the fiber entrance; after the fiber exit; at the end of the spark-plug barrel, just before the final focusing optics; after final focusing optics. Except for the first and last measurement points, some part of the assembly had to be disconnected in order to insert the measuring instrument. For this reason, measurements of multiplexer input energy and of spark-plug output energy could be taken while operating under vacuum, while other measurements were at atmospheric pressure.

5.1.2 Bench-top Control System

As discussed previously, a galvanometer (Cambridge Technology, 6210H) was used to switch the laser beam light between fibers. The galvanometer control board accepted an analog input voltage between -10 V and $+10\text{ V}$, which corresponds to the galvanometer mirror rotating between -20° and $+20^\circ$ from its center position. A LabView program was made (similar to Section 2.2) which could output voltage pulses designed to rotate the galvanometer mirror to the proper position and subsequently fire the laser at the proper time.

This program had added capability from the one in Section 2.2. Whereas the fibers were moved to align with the focal point of the beam during preliminary testing with the galvanometer, for the present bench-top multiplexer testing, the fibers were fixed within the multiplexer, and the beam aligned with them. Horizontal alignment was accomplished via settings within the LabView program, while bulk alignment, as well as alignment in the vertical direction, was done with a yellow paper as described in Section 3.1. Figure 5.1 shows how the computer control system connects to the laser multiplexer and galvanometer.

Even though this program was available, most of the testing described in the following sections was done with the galvanometer pointed at one fiber or the other and the laser being controlled by its own control box. This scheme proved simpler and more useful for the majority of bench-top testing.

5.1.3 Pressure Chamber

A pressure chamber was designed and built in order to test sparking on the bench-top under similar pressure to what is found within the engine cylinder at the time of ignition (i.e. motored pressure at ignition).

Figure 5.2 shows the pressure chamber in assembled and disassembled states.

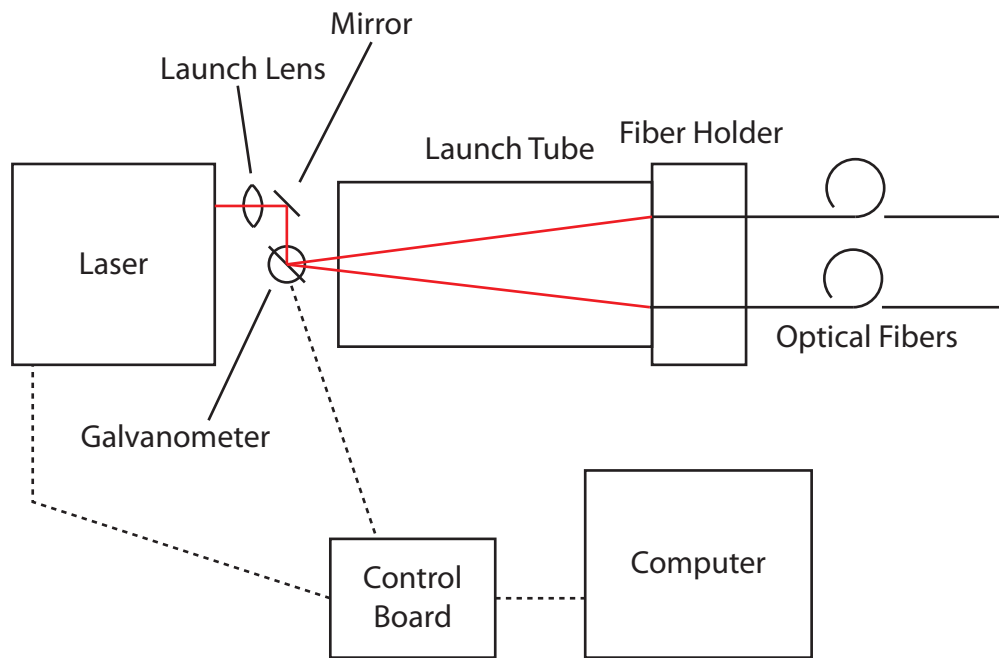


Figure 5.1: Schematic of computer control system for the laser and galvanometer using a control board. The laser beam exits the laser and passes through the launch lens, after which it is reflected 90°, where it hits the galvanometer mirror, and is directed into one of two fibers which are situated in the fiber holder at the end of the launch tube.

The chamber consists of a 4 mm thick glass tube of 3.18 cm diameter, which is sealed at either end with two aluminum plates. Figure A-3.5 in Appendix A-3 shows the nomogram used to decide on a minimum thickness for the glass tube. The glass tube is surrounded by another polycarbonate tube of 5.08 cm diameter, in order to reduce the chance of injury should the glass chamber explode. Everything is held together by six long bolts, surrounding the chamber, spanning from one plate to the other. One plate contained a threaded hole, which was fitted with a quick release gas inlet valve, pressure transducer, pressure release valve, and a safety release valve to prevent overpressure. In the first iteration, the other end plate consisted of two parts sandwiched together with a 2.54 cm x 2 mm thickness sapphire window to provide an aperture with which to aim the spark-plug into the chamber. A minimum thickness of 1.5 mm was calculated using the following equation:

$$t = \sqrt{\frac{1.1pd^2}{m}} \quad (5.1)$$

where t is the thickness of the window, p is the gas pressure of 15.2 bar which compares to the motored pressure at ignition of the Caterpillar 63516C engine, d is the 2.54 cm diameter of the window, and m is the modulus of rupture, which for sapphire is 4,482 bar [49].

The pressure chamber's sapphire window broke on two occasions during initial spark testing. The reason for the breakage is thought to have been a mis-focus of the beam caused by damage to the final focusing lens in the spark-plug, which in turn is thought to have been caused by "hot spots" in the post-fiber beam due to a high M^2 value. After the second breakage of the pressure chamber sapphire window, possibly due to dust within the optical pathway interacting with these "hot spots," a new plate was designed for the pressure chamber, into which the end of the spark-plug could be directly screwed, thus eliminating the problem of the large sapphire window. Once

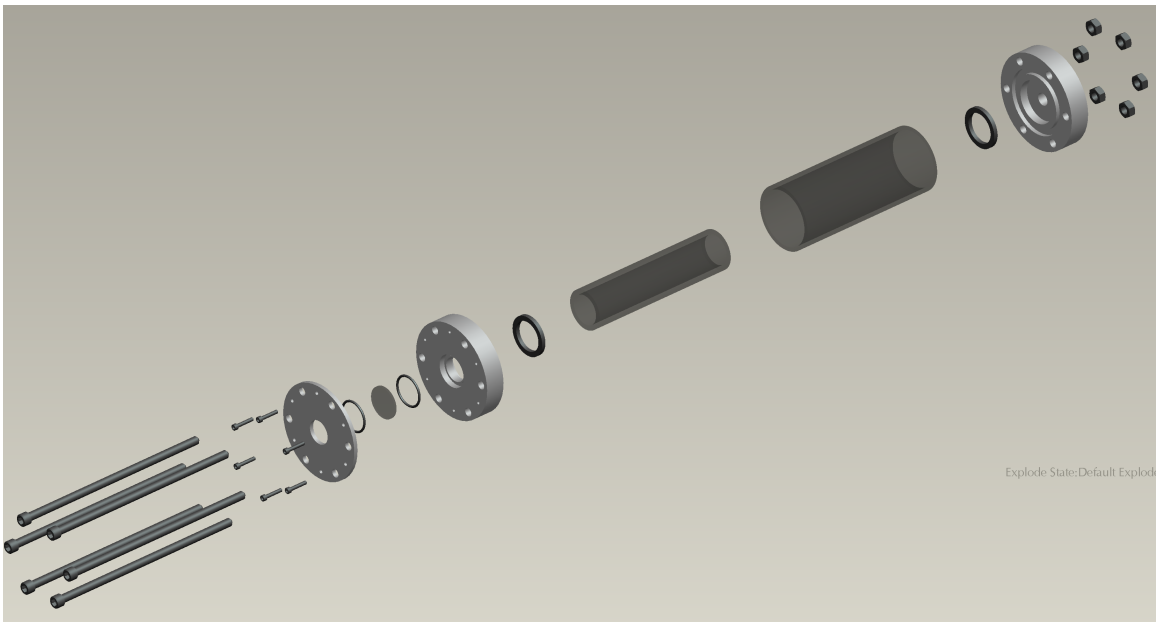
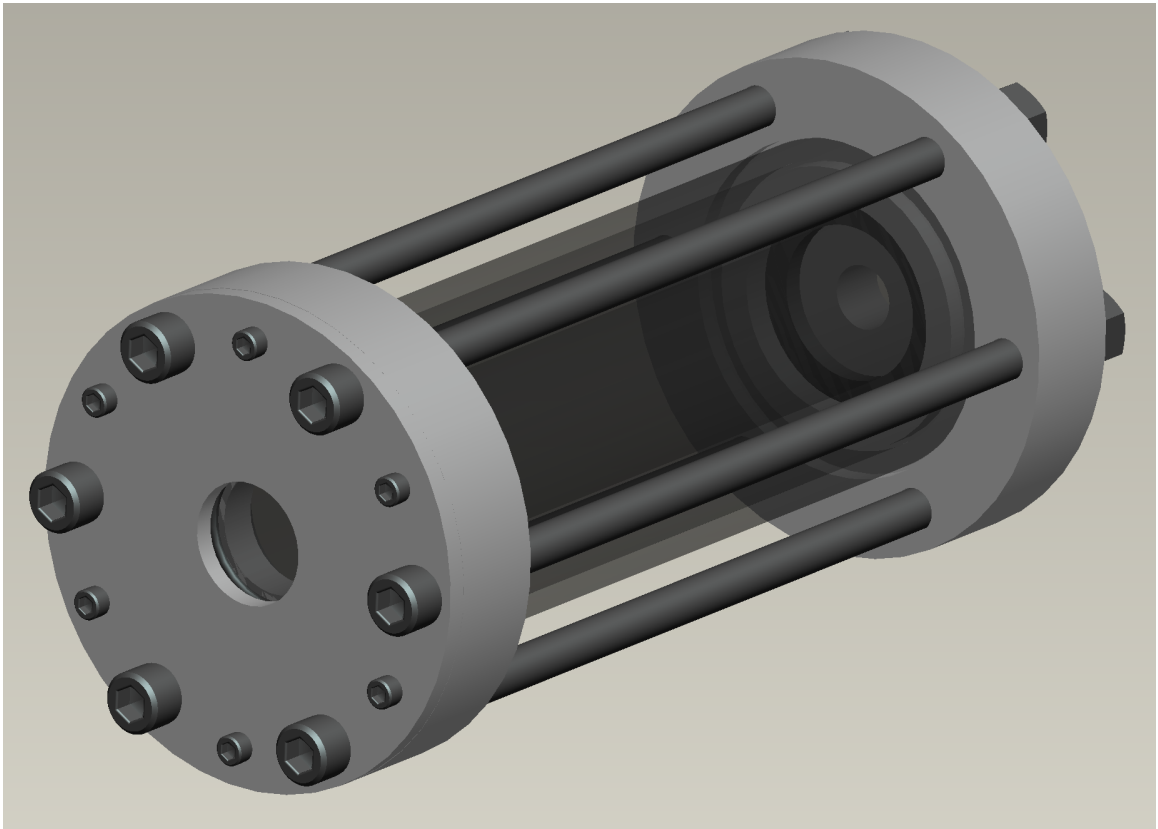


Figure 5.2: The pressure chamber in assembled and disassembled states, showing the glass and polycarbonate tubes, front and back end plates, sapphire window, gaskets and o-rings, and bolts to hold it together.

this was done, sparking tests continued. Appendix A-3 contains technical drawings for some of the pressure chamber parts.

5.1.4 Energy Transmission

First, energy throughput of the individual fiber optics was tested. This was done by measuring the energy just before the fiber but after the galvanometer mirror, E_{in} , and by measuring the energy coming out of the fiber, E_{out} , where $E_{loss} = \frac{E_{in} - E_{out}}{E_{in}}$. The fibers themselves exhibited a loss of 11% to 14%, which is consistent with previous test results of this project [26].

Next, energy throughput at a number of points within the assembly was tested. The energy loss post fiber was found to be $15\% \pm 1.8\%$, which is in accord with the earlier assessment that the damaged galvanometer mirror had caused the significant increase in loss in the previous round of testing. Post collimating lens loss was found to be $19\% \pm 2.2\%$. Post second focusing lens loss was found to be $33\% \pm 1.3\%$.

Table 5.1 shows the predicted energy loss through the system given the measured or rated values of the transmittance of the mirrors, lenses and fibers between the laser opening and the final spark location [50, 51]. In Table 5.1, T_c is the transmittance of a component, L_c is the loss of a component ($1 - T_c$), T_{total} is the total up to and through that component, and L_{total} is the total loss up to and through that component ($1 - E_{trans}$). The relatively high loss of the collimating and final focusing lenses is due to their being uncoated [50]. Hot spots in the post-fiber beam precluded the used of anti-reflection coated optics due to their decreased damage threshold intensity [51].

As can be seen from Table 5.1, the predicted and measured losses through the system coincide well, with an average measured total loss through the system of $33\% \pm 1\%$, compared to a predicted total loss of 31.6%.

Table 5.1: Energy Loss

Location	T_c (%)	L_c (%)	T_{total} (%)	L_{total} (%)	$L_{total,meas}$ (%)
Launch lens	99.50	0.50	99.5	0.5	
90 deg mirror	99.50	0.50	99.0	1.0	
Galvanometer	99.50	0.50	98.5	1.5	
Hollow fiber	87.70	12.30	86.4	13.6	15
Collimating lens	92.50	7.50	79.9	20.1	19
Fist focusing lens	92.50	7.50	73.9	26.1	
Second focusing lens	92.50	7.50	68.4	31.6	33

Predicted energy loss through the system from the laser to a number of different points, given measured or rated values for each component. Where T_c and L_c are the manufacturer specified transmittance and loss of the component, respectively [50–52], T_{total} is the predicted total transmittance up to and through that component, L_{total} is the total loss up to and through that component ($1 - T_{total}$), and $L_{total,meas}$ is the experimentally measured total loss up to and through that component.

5.1.5 Beam Characterization

The beam exiting the fiber was characterized by its measured M^2 value. M^2 was measured for two ~ 2 m fibers as mounted in the multiplexer, with values of the beam diameter taken 10 cm from the end of the fiber. Using strips of burn paper, eleven beam profiles were taken and the diameters roughly measured with a set of digital calipers. Figure 5.3 shows scans of the burn paper strips used for each fiber measurement. Equation 5.2 was used to estimate the M^2 value for each fiber, where w_0 is the 0.5 mm inner radius of the fiber as follows:

$$M^2 = \frac{w_0\pi}{\lambda z} (w(z)^2 - w_0^2)^{1/2} \quad (5.2)$$

where w_0 is the beam waist, λ is the wavelength, z is the distance from the fiber exit to the burn paper, and $w(z)$ is the beam size as measured by the burn paper [47].

For fiber #1, the diameter, assumed to equal twice the beam waist, was found to be 3.54 ± 0.16 mm, which corresponds to an M^2 of 25. For fiber #2, the diameter was

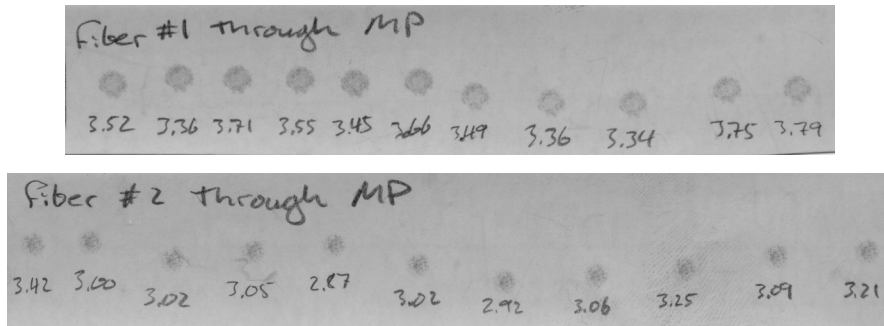


Figure 5.3: Scans of burn papers showing the marks made by the laser for the purpose of determining the M^2 of the beam exiting each fiber. Underneath each mark is written its respective size in mm as measured with calipers.

found to be 3.08 ± 0.15 mm, which corresponds to an M^2 of 22. Previous research at CSU found an M^2 of 11 for 1 m fibers held straight [26]. These results are higher than previously found, but a higher M^2 would be expected for the longer 2 m fibers used in these tests due to the increasing fiber length. Higher M^2 may be due to slight bending of the fibers due to stress imposed by fiber holders and/or unoptimized launch beam diameters at the fiber input.

5.1.6 Sparking Tests

After fixing the problem encountered with the pressure chamber described in Section 5.1.3, short-term sparking tests were conducted according to the following procedure.

The pressure chamber was screwed onto the end of the sparkplug, and pressurized to 15.2 bar (similar to engine motored pressures). The galvanometer was directed to point at a given fiber, and the laser was turned on at its lowest energy level with a firing frequency of 10 Hz. The energy was turned up slowly until regular, near 100% sparking was visible within the pressure chamber. The multiplexer input energy for these tests was measured to be 67 mJ. Given the loss previously measured, of about 33%, the output energy was 45 mJ. The corresponding intensity at the focal spot, based on the beam energy and spacial quality, is $\sim 13000 \text{ GW/cm}^2$, which is consistent

with the expected breakdown intensity at this pressure [7]. The assembly was then maintained in this state for 30 minutes to test the short-term reliability of the system. The system was found to be reliable for the time period tested.

6 Conclusion

6.1 Summary

The goal of this thesis project was to design and build a laser multiplexing system that could produce laser-induced sparks at a motored pressure of 15.2 bar through two hollow-core fiber optics at delivered energies high enough to ignite lean mixtures ($> 10 - 20$ mJ) and at a firing rate sufficient to ignite the 8 cylinders in one bank of a four-stroke Caterpillar G3516C engine running at 1800 rpm (120 Hz). Both solid state and mechanical methods of multiplexing were considered. Solid state methods include the use of electro-optic or acousto-optic modulators combined with other optics to provide very fast and accurate switching of one beam to one of multiple beam output paths. Because of the high cost of the components used in solid state multiplexing, lower cost mechanical methods were also considered. These methods fall into the two categories of *continuous rotation* and the *step-and-hold* approach. The later method, through the use of a galvanometer, was chosen for initial multiplexing tests due to its low cost and ease of use. Initial tests consisted of an 8-channel speed test, and a dual-channel desktop sparking test. Tests were successful, with the galvanometer providing adequate speed for use with 8 channels, and with consistent sparking achieved through both fibers used in the later test.

The design of a multiplexer is subject to the constraints of switching speed and fiber launch accuracy, determined by the speed of the engine and the acceptable error from the central fiber axis when launching the beam into the fiber face, respectively. In discussions with Woodward, a mechanical continuous rotation approach was orig-

inally chosen because of its perceived robustness due to the simple use of a motor. A straight-through axial multiplexer was designed, with the laser at one end, the multiplexer in the middle, and the output fibers exiting parallel to each other at the other end. This was to be accomplished through the use of a parallelogram shaped prism mounted on the shaft of the motor such that a laser beam incident coaxial with the motor exits parallel to, but shifted radially away from, the axis, with the rotational position determined by the rotation of the motor. Woodward was responsible for the software and hardware used to control the motor, but due to logistical reasons, it was decided to switch from the originally designed continuous rotation multiplexer to the previously tested step-and-hold approach with a galvanometer by retrofitting the original design. The final multiplexing method chosen was the step-and hold approach, and included a galvanometer placed at the central axis of the multiplexer, which launched the laser into one of two hollow fibers.

Optical sparkplugs were designed to couple and focus the light exiting the fibers into the combustion chamber. The plug included a 90° turning mirror, such that the fibers enter the plug horizontally, while the exiting light is reflected down into the combustion chamber through a barrel in which was mounted a series of lenses. The light was ultimately focused to a point about 5 mm from the final window face in the end of the plug. Some minor changes were made to the plug during machining and post-machining, with one major change being that the 90° turning mirror was originally designed with no adjustment mechanism. During testing, it was found that this mirror needed adjusting, so a new mounting plate was designed and built, along with the use of a thicker o-ring, to allow for some pointing adjustment of the laser beam.

Multiplexer testing was conducted on the bench-top, with the multiplexer, fibers, and sparkplugs all laid out horizontally. Testing included energy losses through the

multiplexer system, beam M^2 through the fibers, and short-term sparking tests on the bench-top. While a simple control system was created using LabView to synchronize the pointing of the galvanometer with the firing of the laser, most testing was performed by pointing the galvanometer at one channel and firing the laser manually. A pressure chamber was designed and built to attach to the end of the spark-plugs, in order to simulate the pressure within the engine cylinder at the time of ignition. Total energy loss through the multiplexer and sparkplugs was found to be about 31% to 34%, which is consistent with the predicted values. The M^2 of the beams exiting the fibers was found to be 22 to 25, consistent with expected values given the length and slight bending of the fibers. Short-term multiplexer sparking tests at 10 Hz for 30 minutes at 15.2 bar were successful for each channel. Given the results of these tests, the goal of designing, building, and successful bench-top testing of a laser multiplexer system was reached.

6.2 Outlook

Work continuing after this researcher left the laser ignition project at CSU has met with success in using the multiplexer on-engine. With the addition of fine-adjust XY translators for the fibers, and lowering stress on the fibers to reduce mode coupling and achieve lower M^2 at the out of the fiber, more precise beam alignment was made possible. This resulted in 100% sparking in air at atmospheric pressure at input laser energies of 28 mJ. And later, > 99.9% sparking reliability was achieved on-engine at 35 mJ laser input energy and 40% engine load. The laser ignited cylinders suffered from decreased performance versus the spark ignited cylinders. This was found to be due to the fact that the Caterpillar G3516C engine was design for use with pre-chamber style plugs, and thus the in-cylinder environment has much more quiescent flow and combustion, relying on the pre-chamber jets to generate turbulence in the

chamber. This resulted in longer burn durations and lower peak pressure for the laser ignited cylinders due to the lack of turbulence generated by the pre-chamber style spark plug in the spark ignited cylinders. A pre-chamber was added to the laser spark plug, and further tests showed an improvement of the peak pressure in the laser ignited cylinders [53]. However, the pre-chamber laser ignited cylinders still showed decreased peak pressure versus the conventionally ignited cylinders. This is thought to be due to the location of the laser spark within the pre-chamber. The laser spark is located farther into the pre-chamber than the electric sparks, within a more turbulent area, thus causing increased flame stretch and decreased flame growth rate. As of this writing, computational fluid dynamics modeling of the pre-chamber plug is being done to find the best location for the laser spark within the pre-chamber.

Other recent research at CSU has focused on the use of step-index fibers in the use of laser ignition. It was found that increasing the thickness of the cladding improved beam quality by stiffening the core-cladding interface. For example, experiments showed 100% sparking at 10 Hz in atmospheric pressure (0.85 bar) air with 3 to 4 mJ pulse energies through a straight 2 m long fiber with a 200 μm core and 720 μm cladding using a 10 ns pulse of 1064 nm light and a 10 mm focal length lens. When the fiber was bent into a coil with a 25 cm radius, sparking was no longer achievable at atmospheric pressure, but by raising the pressure by just 0.7 bar, 100% sparking was again achieved. This suggests that these step-index fibers should be able to reliably deliver the light necessary for sparks at the high in-cylinder engine pressures. Step-index fibers are not at this time able to transmit the high peak-power to provide the necessary 15 to 20 mJ required for ignition with 10 ns laser pulse widths, so further research is being conducted on widening the laser pulse widths (and therefore lower the peak power in the fibers), as well as using multiple pulses a short time apart (~ 40 ns) [33], in order to deliver the needed ignition energy.

In the near term, future work should also include further refinements to the multiplexer system as more testing is conducted. Due to the very strict tolerances required to implement a continuous rotation multiplexer, a step-and-hold galvanometer-based approach should remain the multiplexing method, because it allows for a maximum of adjustability. This includes designing and building a new multiplexer to better incorporate a dual-axis galvanometer-based system. This dual-axis system would allow for both horizontal and vertical aiming adjustment for each fiber channel on an individual basis. Fibers could then be fixed in whatever arrangement desired based on the intended multiplexing application. In the case of this work, the ideal fiber pattern would probably be in a circle, such that consecutive fibers in the circle would fire the engine cylinders in the correct order. While a circle might be the ideal pattern, a straight horizontal line of fibers might prove easier to manufacture, with the vertical axis galvanometer serving to adjust for minor positioning differences between fibers. If switching time is a concern, the fibers could be interleaved such that the multiplexer would only have to switch a distance of two fibers at any one time, instead of making a large jump from the fiber at one end of the line to the fiber at the other end. See Figure 6.1 for a diagram of these fiber patterns as well as their switching order variations.

In the longer term, the drawbacks of the hollow fibers used in this work may be challenging for moving laser ignition from the research to the industrial sector. First, the fiber damage threshold, which is only slightly higher than the energy required for laser ignition under, means that the fibers tend to become damaged after extended use, due to sporadic damage at the entrance and within, caused by any slight misalignment or by any dust or dirt which happens to drift by, or which has been deposited on the fiber through handling. Second, the fibers have a very limited capacity for bending, due to two factors: the fibers themselves can only bend at a

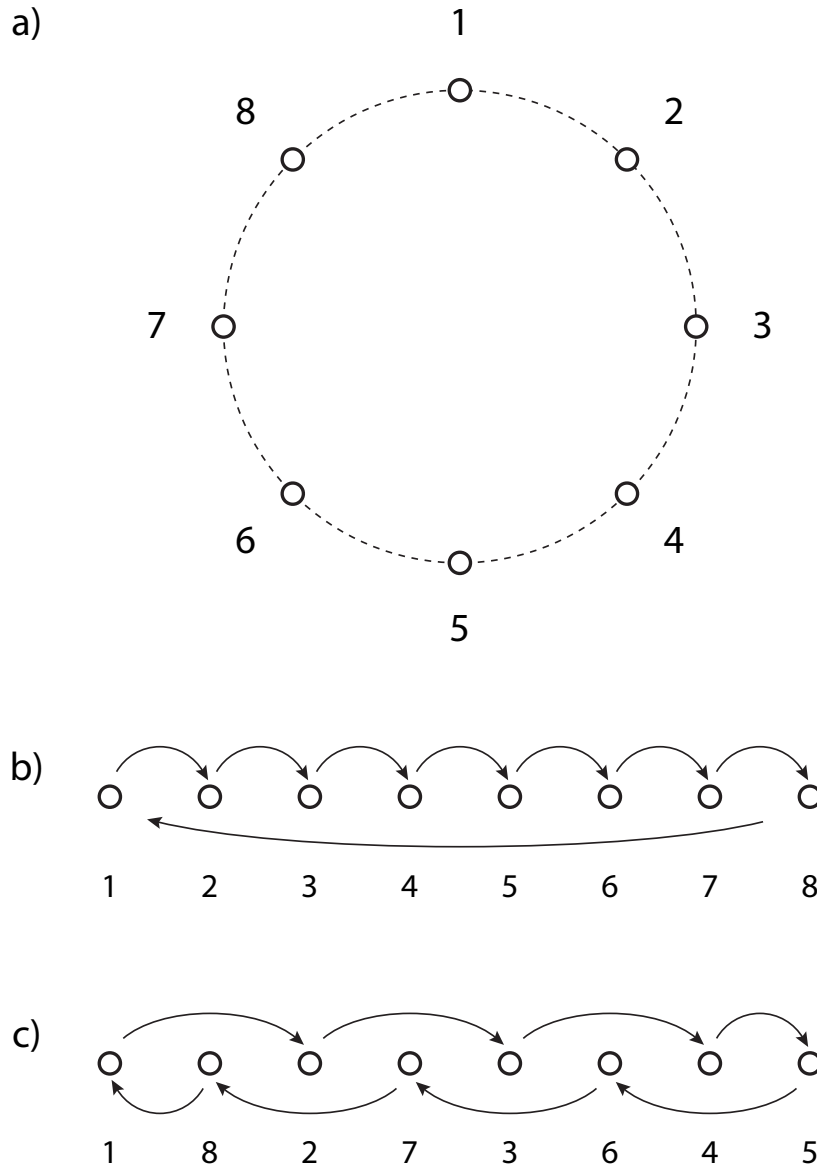


Figure 6.1: Diagrams of possible fiber switching patterns where the small circles are the fiber faces, the numbers are the switching order, and the arrows illustrate the switching pattern. a) is the circular switching pattern, which provides exactly the same distance between each switching jump; b) is the straight pattern where the laser goes to the next fiber in turn, then jumps from the last fiber back to the first; and c) is the interleaved straight pattern, where the maximum jump distance for the laser is only two fiber positions.

large radius without breaking, and a significant loss of beam quality occurs when the fibers are bent. Further research is needed to address reliability and lifetime. Other research has considered designs allowing practical access to multiple engine cylinders with minimal bending.

One potential solution to these problems with hollow fibers would be a move to a fiber-laser based system. Since this system would essentially have one fiber laser per cylinder, with the pump light delivered via a multiplexer, the problems associated with introducing a short but very high intensity pulse into a fiber are eliminated, because the pump light can be easily multiplexed due to its much lower intensity and longer pulse duration. At this time fiber laser technology is moving towards producing the energy required to ignite a combustible mixture, and usable results are likely to be achieved within a few years.

A second potential solution may be based on current work at CSU using step-index fibers with large dimension cladding.

References

- [1] Lackner, M., Winter, F., Graf, J., Geringer, B., Weinrotter, M., Kopecek, H., Wintner, E., Klausner, J., and Herdin, G., 2004. “Laser ignition in internal combustion engines - a contribution to a sustainable environment”. In Proceedings of the 14th International Flame Reserch Foundation Members’ Conference.
- [2] Kopecek, H., Maier, H., Reider, G., Winter, F., and Wintner, E., 2003. “Laser ignition of methane–air mixtures at high pressures”. *Experimental Thermal and Fluid Science*, **27**, pp. 499–503.
- [3] Heywood, J. B., 1988. *Internal combustion engine fundamentals*. McGraw-Hill international editions.
- [4] Ronney, P. D., 1994. “Laser versus conventional ignition of flames”. *Optical Engineering*, **33**(2), February, pp. 510–521.
- [5] Dale, J. D., Smy, P. R., and Clements, R. M., 1978. Laser ignited internal combustion engine – an experimental study. SAE Paper No. 780329, Society of Automotive Engineers.
- [6] Weinrotter, M., Kopecek, H., Wintner, E., Lackner, M., and Winter, F., 2005. “Application of laser ignition to hydrogen–air mixtures at high pressures”. *International Journal of Hydrogen Energy*, **30**, pp. 319–326.

- [7] Phuoc, T. X., 2000. “Laser spark ignition: experimental determination of laser-induced breakdown thresholds of combustion gases”. *Optics Communications*, **175**, pp. 419–423.
- [8] Stakhiv, A., Gilber, R., Kopecek, H., Zheltikov, A. M., and Wintner, E., 2004. “Laser ignition of engines via optical fibers?”. *Laser Physics*, **14**(5), pp. 738–747.
- [9] Turcu, I. C. E., Gower, M. C., and Huntington, P., 1997. “Measurement of krf laser breakdown threshold in gases”. *Optics Communications*, **134**(1-6), pp. 66–68.
- [10] Rosen, D. I., and Weyl, G., 1987. “Laser-induced breakdown in nitrogen and the rare gases at 0.53 and 0.357 μm ”. *Journal of Physics D: Applied Physics*, **20**(10), pp. 1264–1276.
- [11] Ma, J. X., Alexander, D. R., and Poulain, D. E., 1998. “Laser spark ignition and combustion characteristics of methane-air mixtures”. *Combustion and Flame*, **112**, pp. 492–506.
- [12] Yalin, A. P., Defoort, M. W., Joshi, S., Olsen, D., Willson, B., Matsuura, Y., and Miyagi, M., 2005. “Laser ignition of natural gas engines using fiber delivery”. In Proceedings of ICEF2005: ASME Internal Combustion Engine Division 2005 Fall Technical Conference, no. ICEF 2005-1336.
- [13] Weinrotter, M., Kopecek, H., Wintner, E., Lackner, M., and Winter, F., 2003. “Laser ignition of hydrogen-air mixtures at high pressures”. In Proceedings of the European Combustion Meeting, European Combustion Institute.
- [14] Ma, J. X., III, T. W. R., and Buckingham, J. P., 1998. “Nd:yag laser ignition of natural gas”. In ASME Spring Technical Conference, no. 98-ICE-114.

- [15] Herdin, D. G., Klausner, D. J., Weinrotter, D. M., Graf, D. J., and Wimmer, D. A., 2006. “Ge jenbacher’s update on laser ignited engines”. In Proceedings of ICEF2006: ASME Internal Combustion Engine Division 2006 Fall Technical Conference, no. ICEF 2006-1547.
- [16] Herdin, D. G., Klausner, D. J., Wintner, P. E., Weinrotter, D. M., Graf, J., and Iskra, K., 2005. “Laser ignition - a new concept to use and increase the potentials of gas engines”. In Proceedings of ICEF2005: ASME Internal Combustion Engine Division 2005 Fall Technical Conference, no. ICEF 2005-1352.
- [17] Phuoc, T. X., 2000. “Single-point versus multi-point laser ignition: experimental measurements of combustion times and pressures”. *Combustion and Flame*, **122**(4), pp. 508–510.
- [18] Morsy, M. H., Ko, Y. S., Chung, S. H., and Cho, P., 2001. “Laser-induced two-point ignition of premixture with a single-shot laser”. *Combustion and Flame*, **124**(4), pp. 724–727.
- [19] Morsy, M. H., and Chung, S. H., 2003. “Laser-induced multi-point ignition with a single-shot laser using two conical cavities for hydrogen/air mixture”. *Experimental Thermal and Fluid Science*, **27**(4), pp. 491–497. Second Mediterranean Combustion Symposium.
- [20] McMillian, M. H., Woodruff, S. D., Richardson, S. W., and McIntyre, D. L., 2004. “Laser spark ignition: Laser development and engine testing”. In Proceedings of ICEF2004, ASME Internal Combustion Engine Division 2004 Fall Technical Conference, no. ICEF 2004-917 in Paper No.

- [21] Kofler, H., Tauer, J., Tartar, G., Iskra, K., Klausner, J., Herdin, G., and Wintner, E., 2007. “An innovative solid-state laser for engine ignition”. *Laser Physics Letters*, **4**, pp. 322–327.
- [22] Kroupa, G., Franz, G., and Winkelhofer, E., 2009. “Novel miniaturized high-energy nd-yag laser for spark ignition in internal combustion engines”. *Optical Engineering*, **48**(1), January, pp. 14202–1–14202–5.
- [23] Tsunekane, M., Inohara, T., Ando, A., Kanehara, K., and Taira, T., 2008. “High peak power, passively q-switched cr:yag/nd:yag micro-laser for ignition of engines”. In *Advanced Solid-State Photonics*, Optical Society of America, p. MB4.
- [24] Ctr carinthian tech research ag - high power laser: diminutive size - huge potential. On the WWW at http://www.ctr.at/carinthian_tech_research_deutsch/dokumente/Daten_u_Produktblaetter/optSysteme/folder_hipolas_web_v01.pdf.
- [25] Paschotta, R., 2008. *Encyclopedia of Laser Physics and Technology*. Wiley-VCH, ch. M2 Factor. On the WWW at http://www.rp-photonics.com/m2_factor.html.
- [26] Yalin, A. P., DeFoort, M., Willson, B., Matsuura, Y., and Miyagi, M., 2005. “Use of hollow-core fibers to deliver nanosecond nd: Yag laser pulses to form sparks in gases”. *Optics Letters*, **30**(16), pp. 2083–2085.
- [27] Matsuura, Y., Hanamoto, K., Sato, S., and Miyagi, M., 1998. “Hollow-fiber delivery of high-power pulsed nd:yag laser light”. *Optics Letters*, **23**(23), pp. 1858–1860.

- [28] Matsuura, Y., Takada, G., Yamamoto, T., Shi, Y.-W., and Miyagi, M., 2002. “Hollow fibers for delivery of harmonic pulses of q-switched nd:yag lasers”. *Applied Optics*, **41**(3), pp. 442–445.
- [29] Sato, S., Ashida, H., Shi, Y.-W., Matsuura, Y., and Miyagi, M., 1999. “Hollow-waveguide-based transmission of a q-switched nd:yag laser beam for biological tissue ablation”. A. Katzir and J. A. Harrington, eds., Vol. 3596, SPIE, pp. 50–54.
- [30] Sato, S., Ashida, H., Arai, T., Shi, Y.-W., Matsuura, Y., and Miyagi, M., 2000. “Vacuum-cored hollow waveguide for transmission of high-energy, nanosecond nd:yag laser pulses and its application to biological tissue ablation”. *Optics Letters*, **25**(1), pp. 49–51.
- [31] Cheng, M.-Y., Chang, Y.-C., Galvanauskas, A., Mamidipudi, P., Changkakoti, R., and Gatchell, P., 2005. “High-energy and high-peak-power nanosecond pulse generation with beam quality control in 200-um core highly multimode yb-doped fiber amplifiers”. *Optics Letters*, **30**(4), February, pp. 358–360.
- [32] El-Rabii, H., and Gaborel, G., 2007. “Laser ignition of flammable mixtures via a solid core optical fiber”. *Applied Physics B: Lasers and Optics*, **87**(1), March, pp. 139–144.
- [33] Yalin, A., Loccisano, F., Joshi, S., Zhang, Z., and Shneider, M., 2010. “Pre-ionization controlled laser plasma formation for ignition applications”. In Proceedings of the 41st Plasmadynamics and Lasers Conference, no. AIAA 2010-4307.

- [34] Joshi, S., Yalin, A., D'Angola, A., Colonna, G., Puzinauskas, C. D. P. V., and El-Rabii, H., 2010. "A time resolved spectroscopic study of laser generated plasmas in air at high pressures". In Proceedings of the 41st Plasmadynamics and Lasers Conference, no. AIAA 2010-4309.
- [35] Paschotta, R., 2008. *Encyclopedia of Laser Physics and Technology*. Wiley-VCH, ch. Electro-optic Modulators. On the WWW at http://www.rp-photonics.com/electro_optic_modulators.html.
- [36] Early, J. W., and Lester, C. S., 1999. *Optical Fiber Switch*. U. S. Patent Office, February. Patent number 6,351,579.
- [37] CLEVELAND CRYSTALS. *IMPACT Series KD*P Pockels Cell*. On the WWW at <http://www.clevelandcrystals.com/IMPACT/IMPACT\%20datasheet\%2006.pdf>.
- [38] CVI MELLES GRIOT. *High Energy Laser Line Polarizing Cube Beamsplitters*. On the WWW at http://www.cvimellesgriot.com/products/Documents/TechnicalGuide/Antireflection_Coatings_CVIMG.pdf.
- [39] CVI MELLES GRIOT. *High Power Nd:YAG Laser Mirrors*. On the WWW at http://www.cvimellesgriot.com/products/Documents/TechnicalGuide/Antireflection_Coatings_CVIMG.pdf.
- [40] United Crystals Company, 2010. Quote for dkdp pockels cell, aperture 10mm, with ar-coated dkdp crystal and bk-7 windows (outer diameter 25.0mm). private communication.

- [41] Paschotta, R., 2008. *Encyclopedia of Laser Physics and Technology*. Wiley-VCH, ch. Acousto-optic Modulators. On the WWW at http://www.rp-photonics.com/acousto_optic_modulators.html.
- [42] GOOCH & HOUSEGO. *Industry Standard Acousto-Optic Q-Switch*. On the WWW at <http://www.goochandhousego.com/sites/default/files/documents/Industry%20standard%20Q-Switch%20data%20sheet.pdf>.
- [43] Gooch & Housego, 2010. Quote for 45035-5-6.5deg-1.06 acousto-optic modulator and 31035-4ds driver. private communication.
- [44] Thorlabs catalog: Modular piezoelectric actuators. On the WWW at <http://www.thorlabs.com/catalogPages/291.pdf>.
- [45] Cambridge Technology, 2010. Quote for 6210h galvanometer with 6mm ya x mounted mirror and 671xx servo driver amplifier. private communication.
- [46] MELLES GRIOT, 2002. *Melles Griot Optics Guide*. On the WWW at <http://www.mellesgriot.com/products/optics/toc.htm>.
- [47] Verdeyen, J. T., 2000. *Laser Electronics*, third ed. Prentice Hall, Upper Saddle River, New Jersey.
- [48] Siegman, A. E., and Townsend, S. W., 1993. "Output beam propagation and beam quality from a multimode stable-cavity laser". *IEEE Journal of Quantum Electronics*, **29**(4), pp. 1212–1217.
- [49] Isp optics: Design of pressure window. On the WWW at <http://www.ispoptics.com/DesignOfPressureWindow.htm> and http://www.ispoptics.com/PDFs/optical_design.pdf.
- [50] Thorlabs catalog. On the WWW at <http://www.thorlabs.com/>.

- [51] CVI MELLES GRIOT. *Antireflection Coatings*. On the WWW at http://www.cvimellesgriot.com/products/Documents/TechnicalGuide/Antireflection_Coatings_CVIMG.pdf.
- [52] Cvi melles griot. On the WWW at <http://www.cvimellesgriot.com/>.
- [53] Joshi, S., Loccisano, F., Yalin, A., and Montgomery, D., (accepted) 2010. “On comparative performance testing of prechamber and open chamber laser ignition”. In ASME Internal Combustion Engine Fall Technical Conference, no. ICEF 2010-35058.

A-1 Multiplexer technical drawings

All technical drawings made for the multiplexer are shown below. Not all parts of the multiplexer were illustrated, because Woodward, who did most of the machining for the multiplexer, referenced the source Pro/Engineer files directly to build many of the parts.

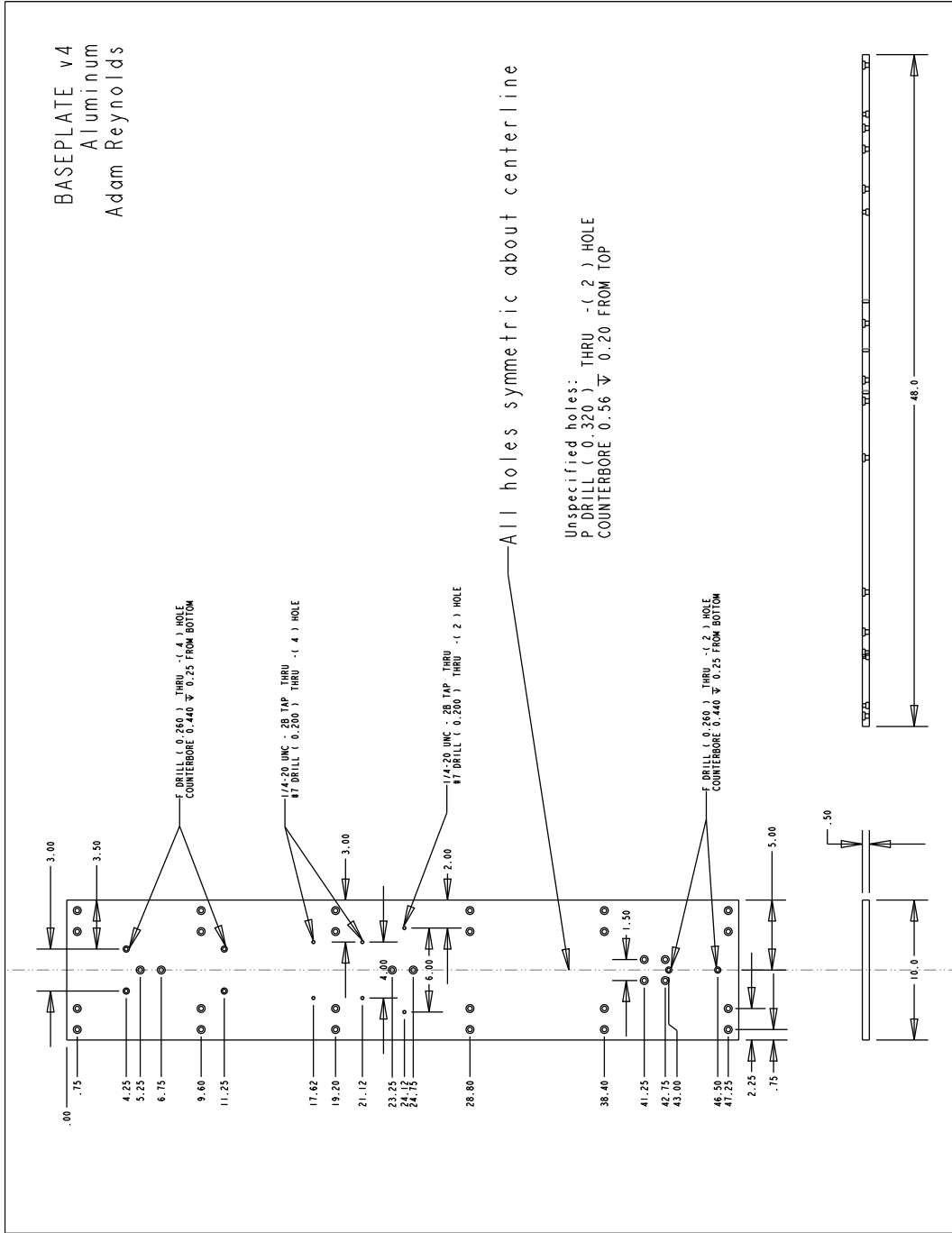


Figure A-1.1: Baseplate.

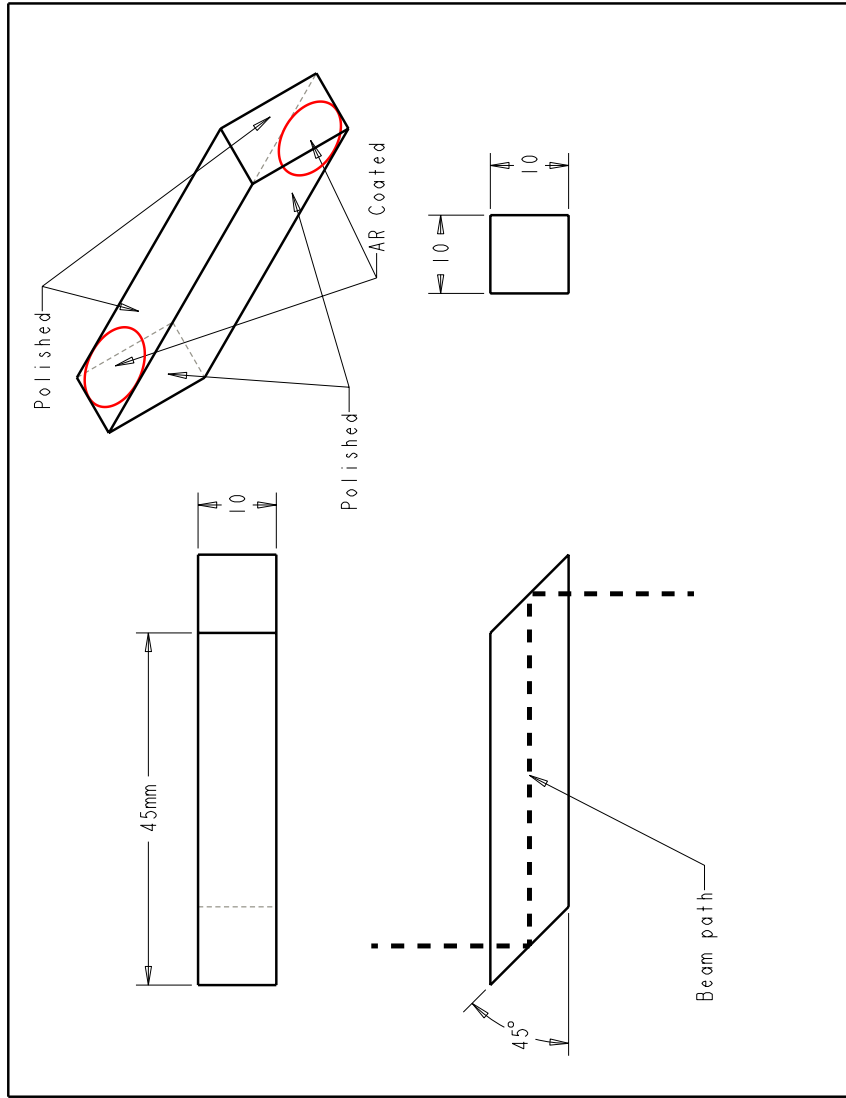


Figure A-1.2: Prism.

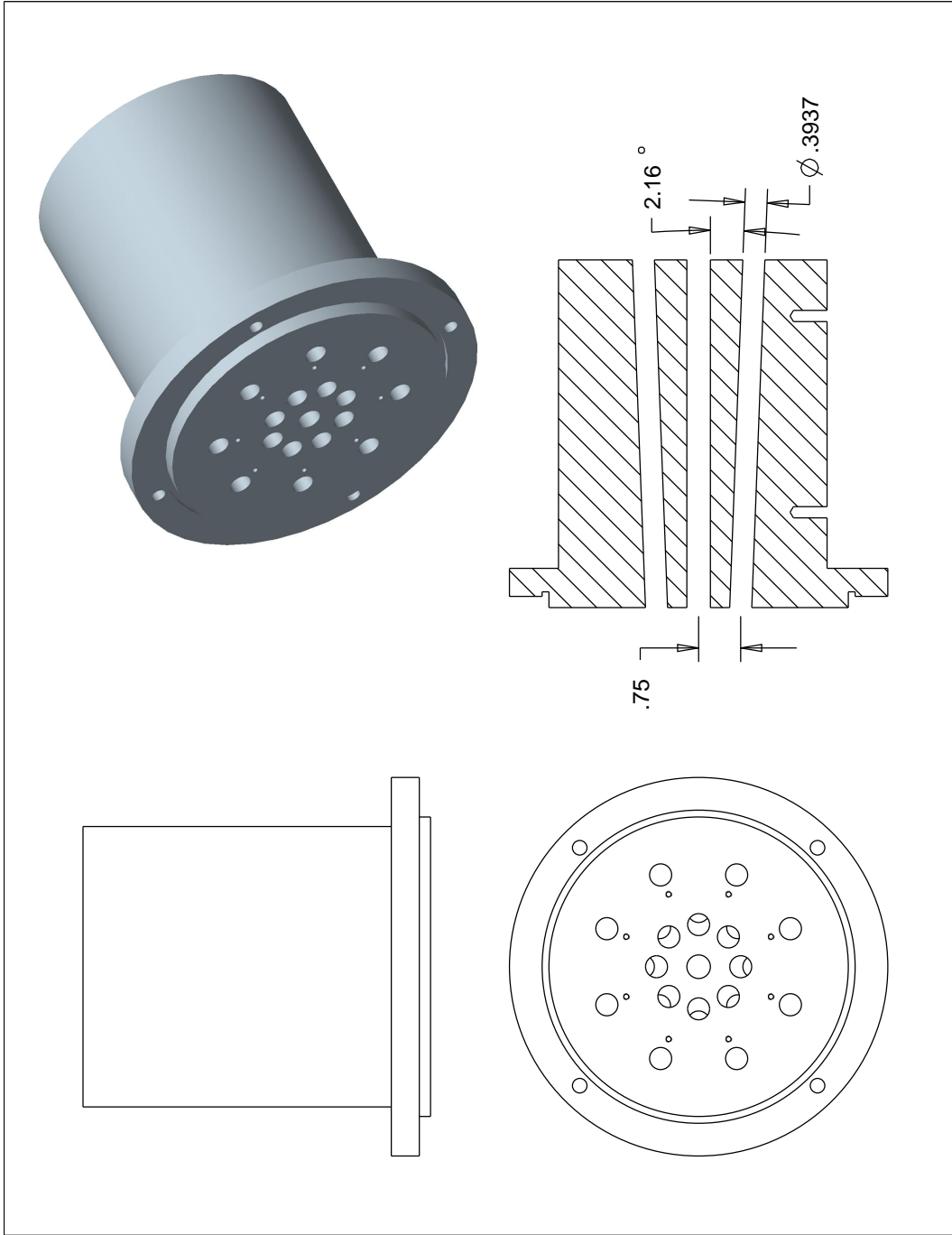


Figure A-1.3: Fiber holder.

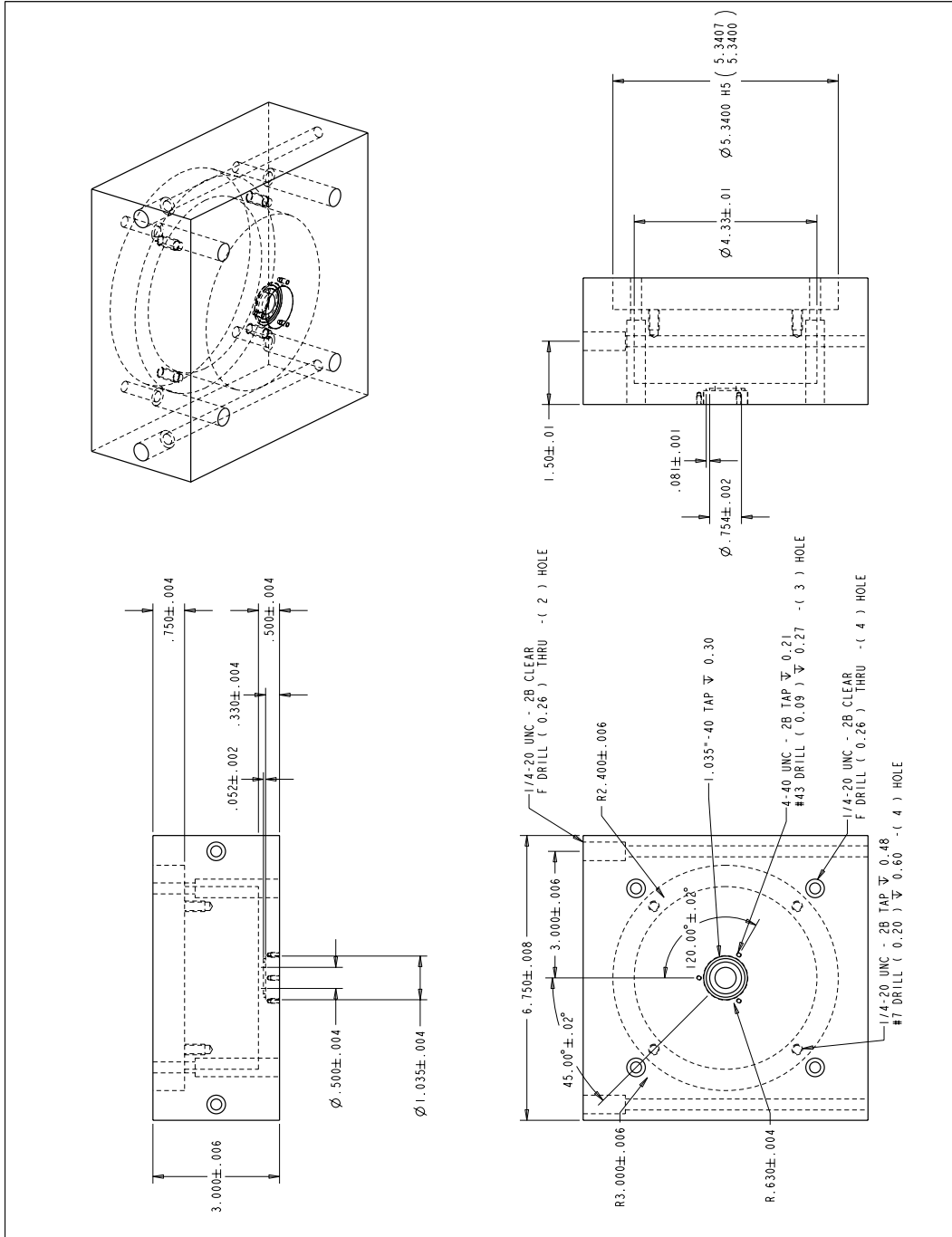


Figure A-1.4: Front attachment.

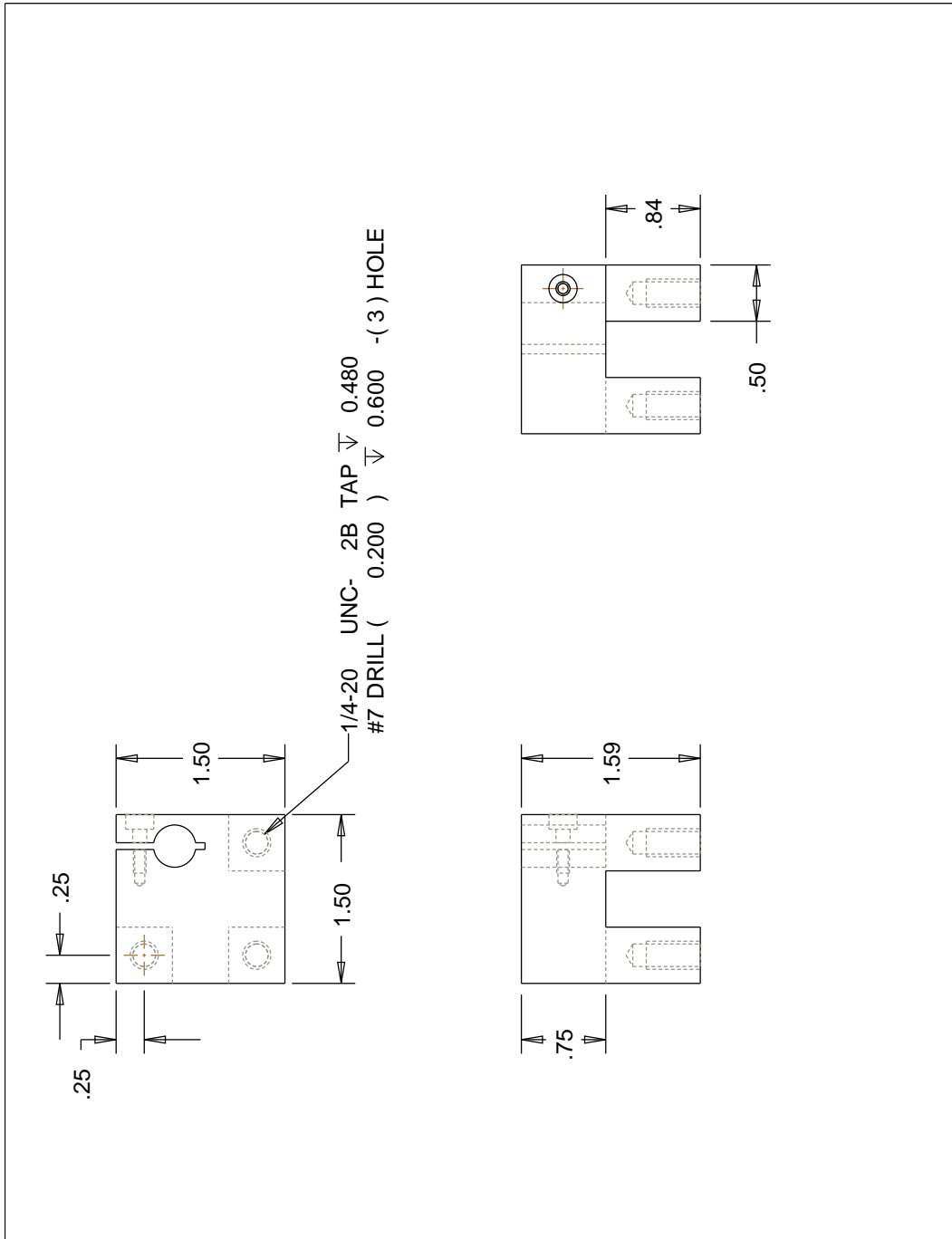


Figure A-1.5: Galvanometer mounting block.

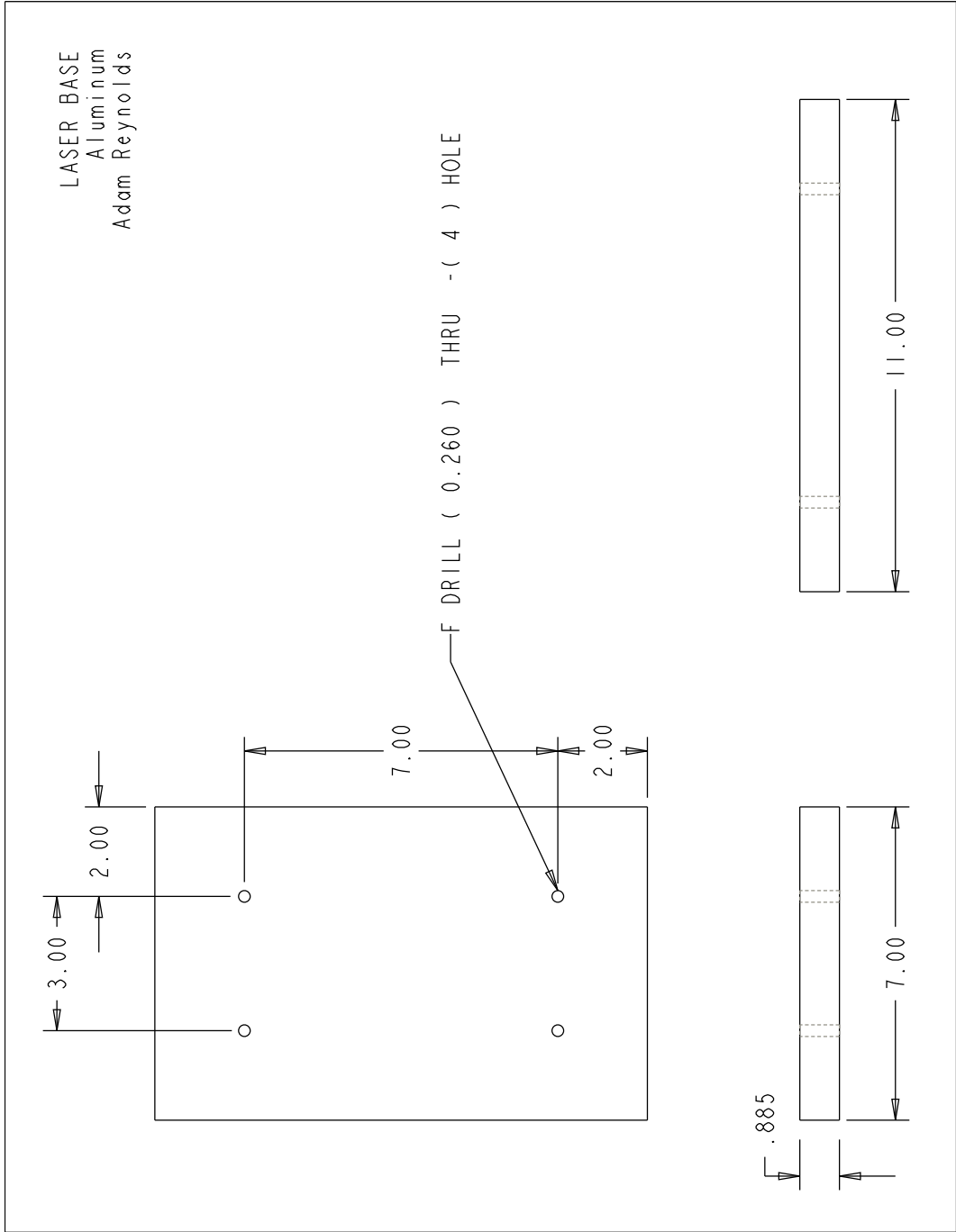


Figure A-1.6: Laser base.

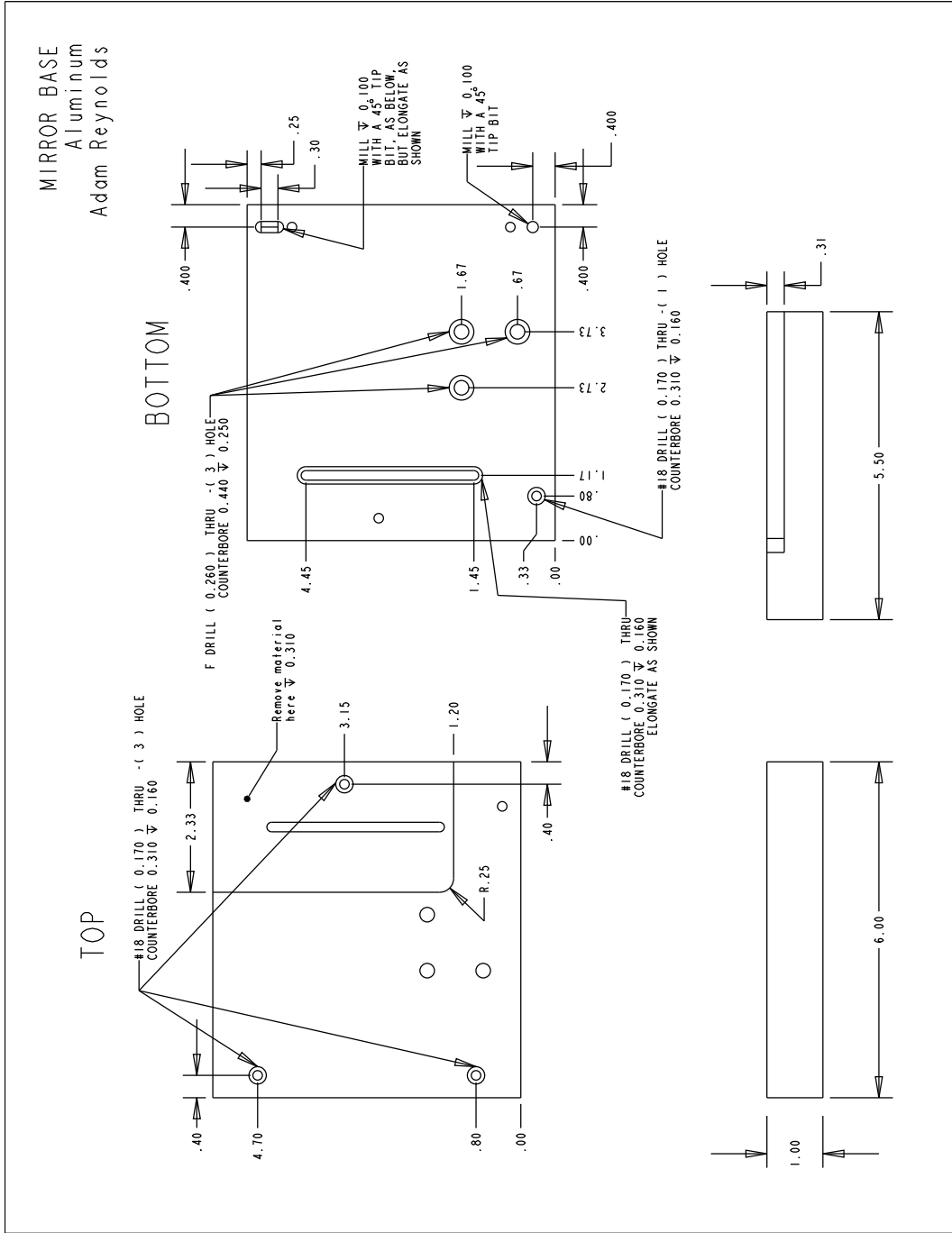


Figure A-1.7: Mirror base.

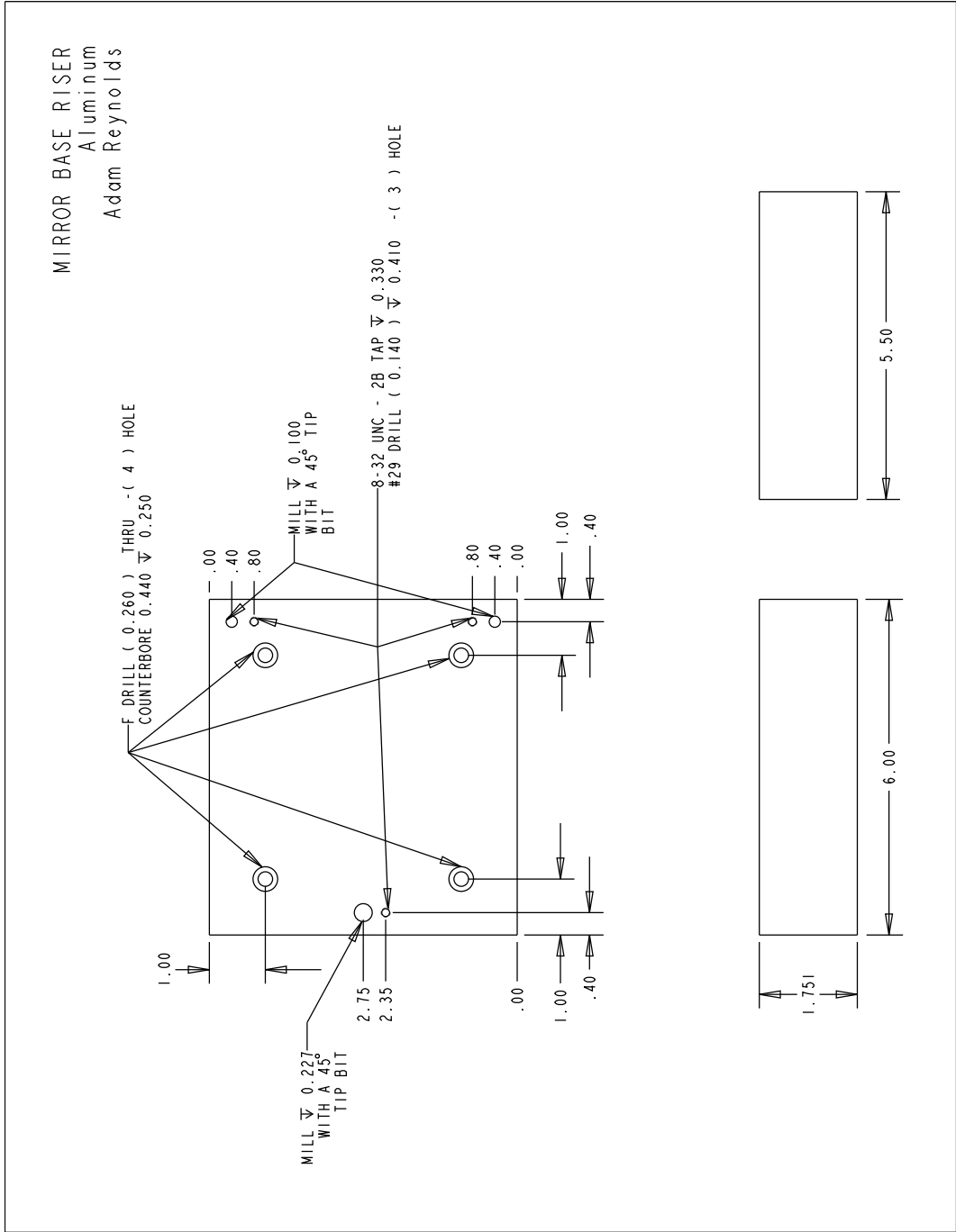


Figure A-1.8: Mirror base riser.

FIBER HOLDER MOUNTING BLOCK
 Aluminum
 Adam Reynolds

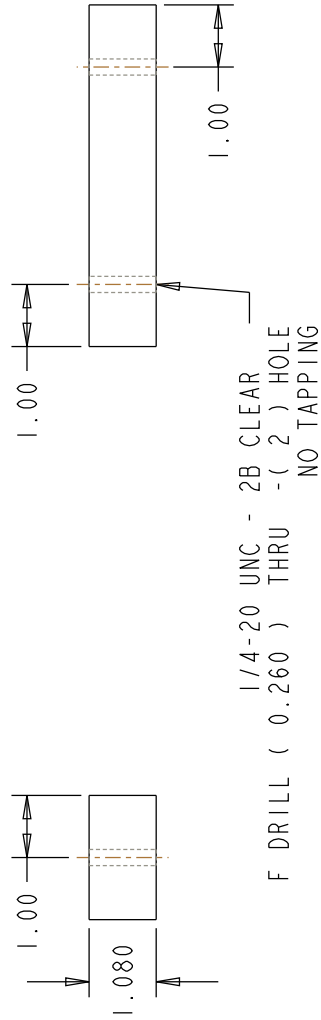
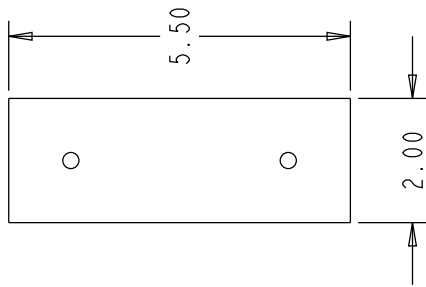


Figure A-1.9: Fiber holder mounting block riser.

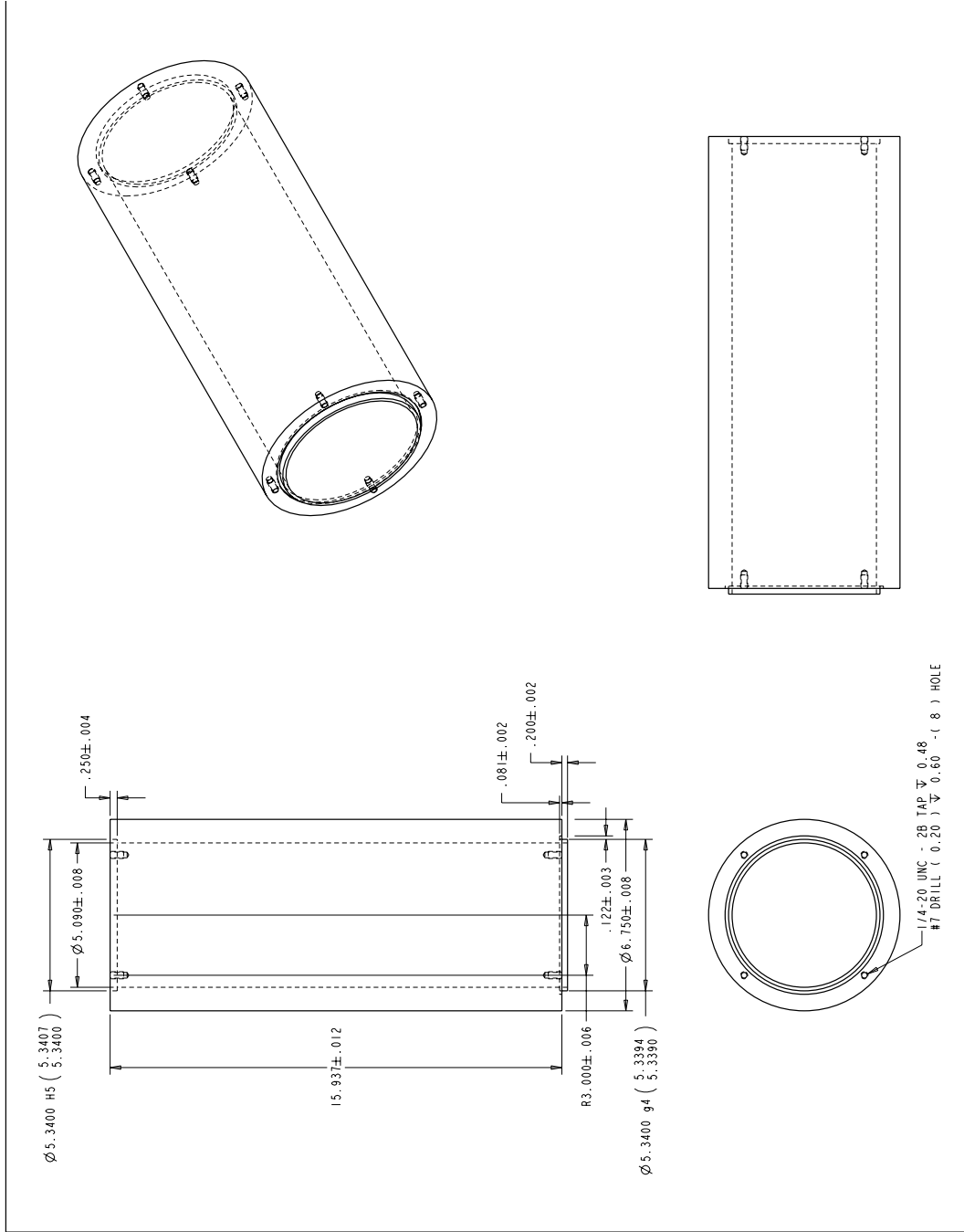
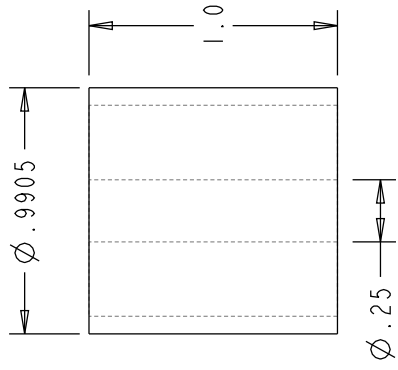


Figure A-1.10: Launch tube.

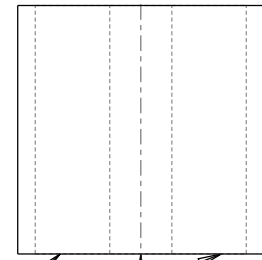
A-2 Sparkplug technical drawings

All technical drawings made for the sparkplug are shown below. Again, Woodward, who did the machining for the sparkplugs, worked from the original Pro/Engineer files, so not all sparkplug parts are represented.

ADAPTER PLUG
 Aluminum
 Adam Reynolds
 Project 533832
 Make 2x PIECES



2 dowel holes on either side of NPT tapping
 to fit EXTRACTOR piece



1/4 NPT TAPPING
 from one end

1-8 UNC 2B THREAD
 along outer length

Figure A-2.1: Adapter plug.

CHUCK HOLDER
Aluminum
Adam Reynolds
Project 533832
Make 2x PIECES

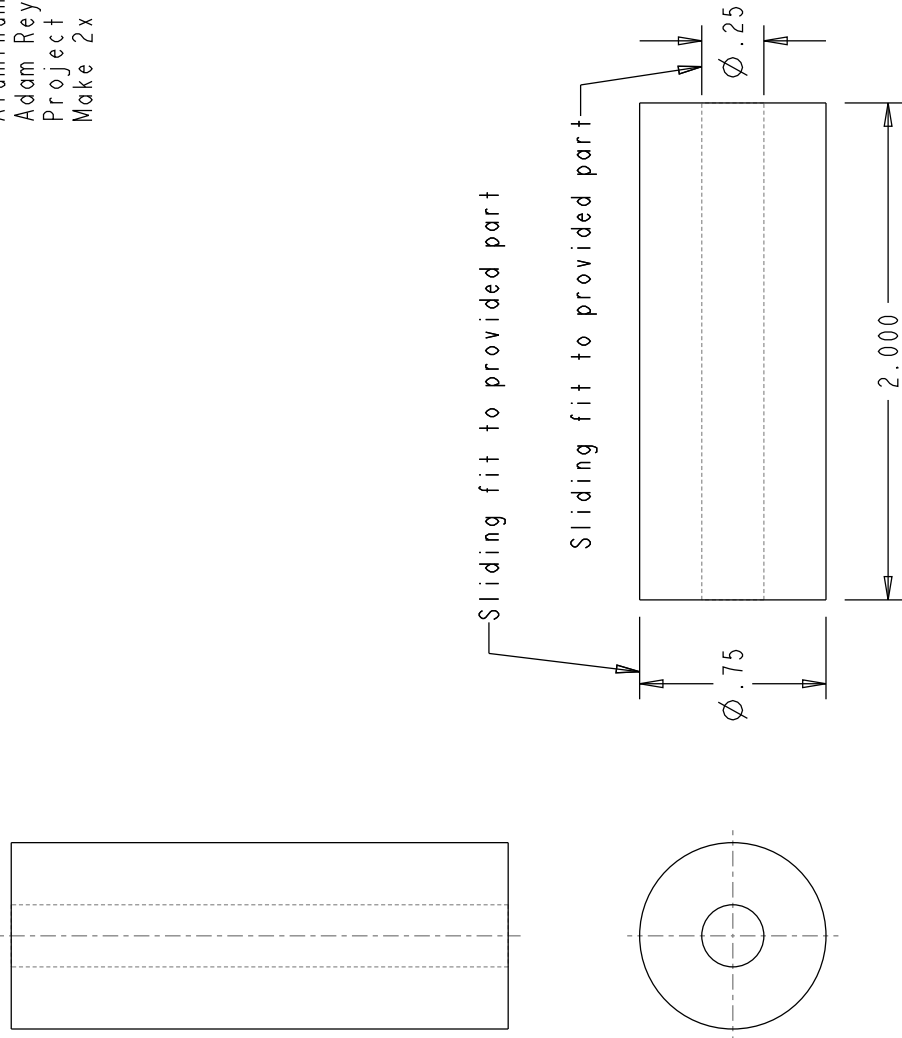


Figure A-2.2: Chuck holder.

HEAD modification
Adam Reynolds
Project #533832
QTY: 2

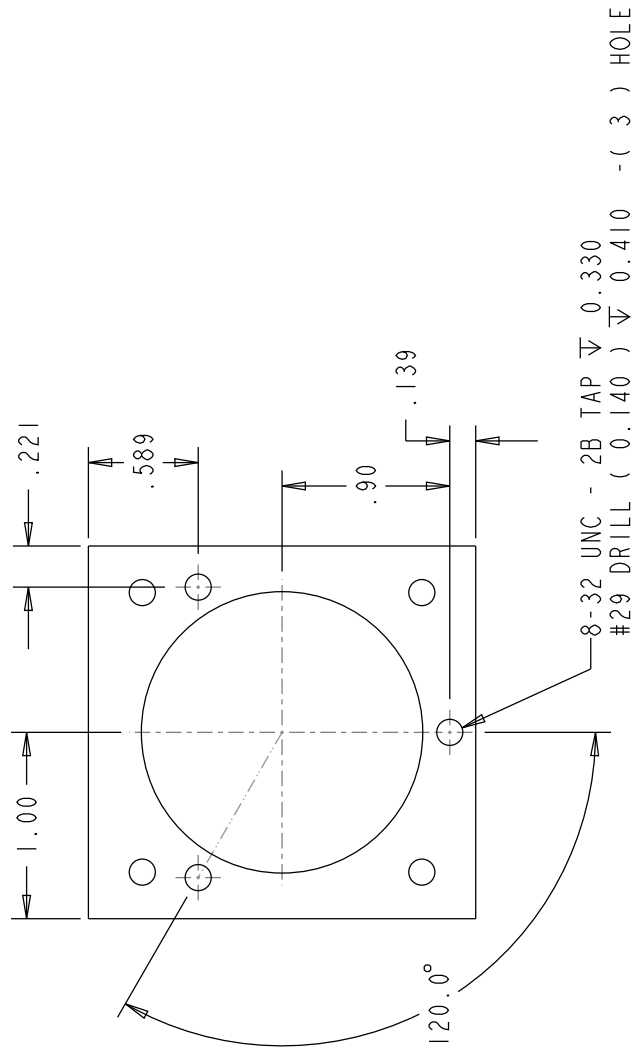


Figure A-2.3: Head modification.

MIRROR CLAMP v2
Adam Reynolds
Project #533832
Stainless Steel
QTY: 2

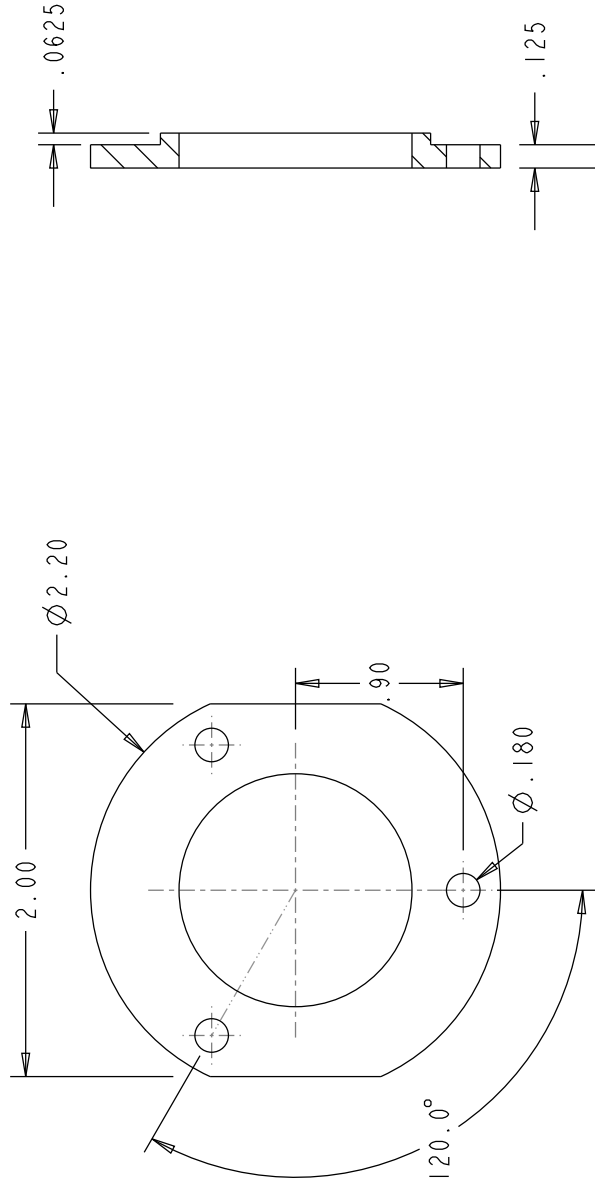
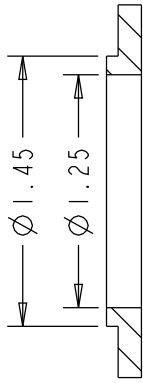


Figure A-2.4: Second mirror clamp.

A-3 Pressure chamber technical drawings

Below are the technical drawings used to machine the pressure chamber in which the multiplexer and optical sparkplug systems were tested.

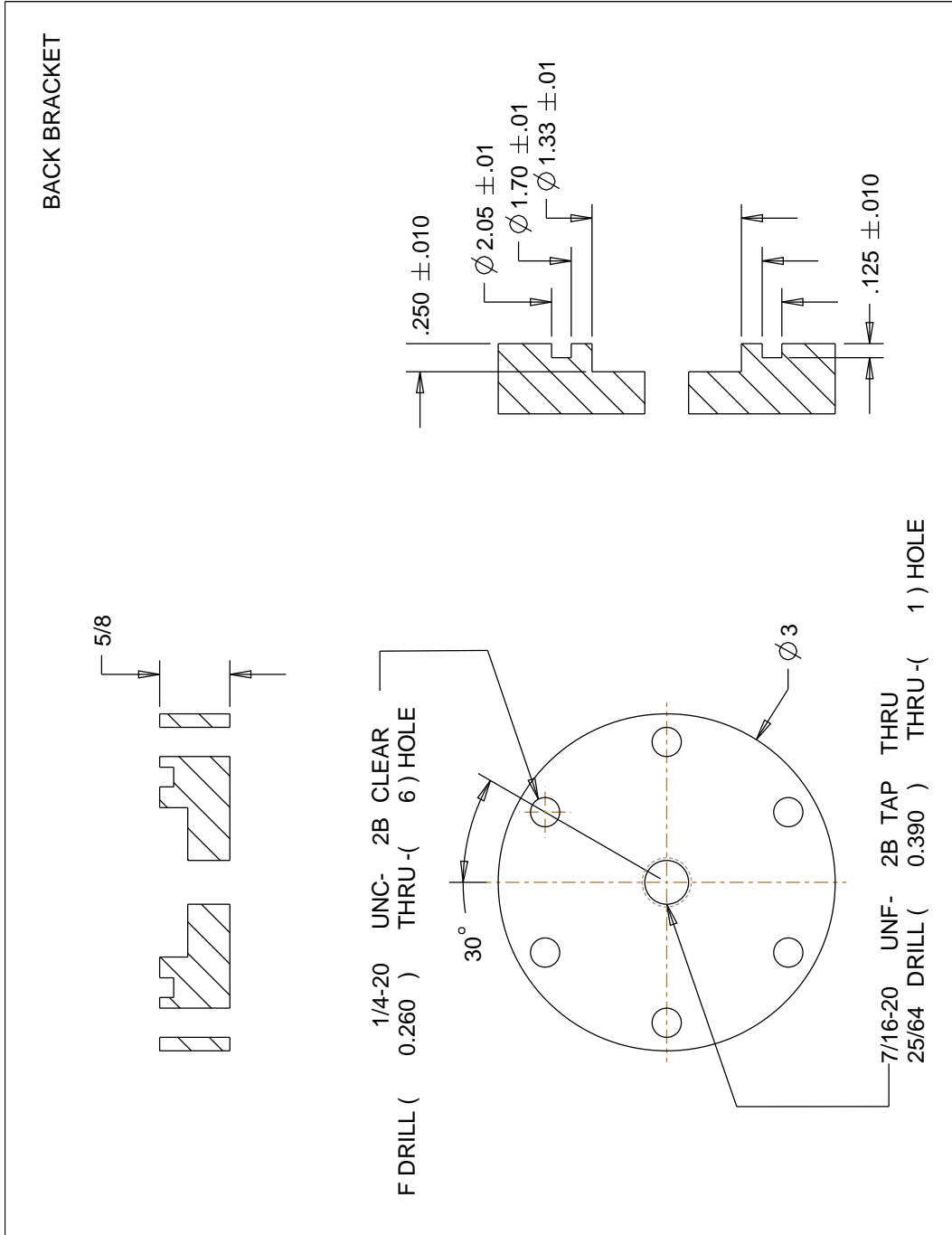


Figure A-3.1: Back bracket.

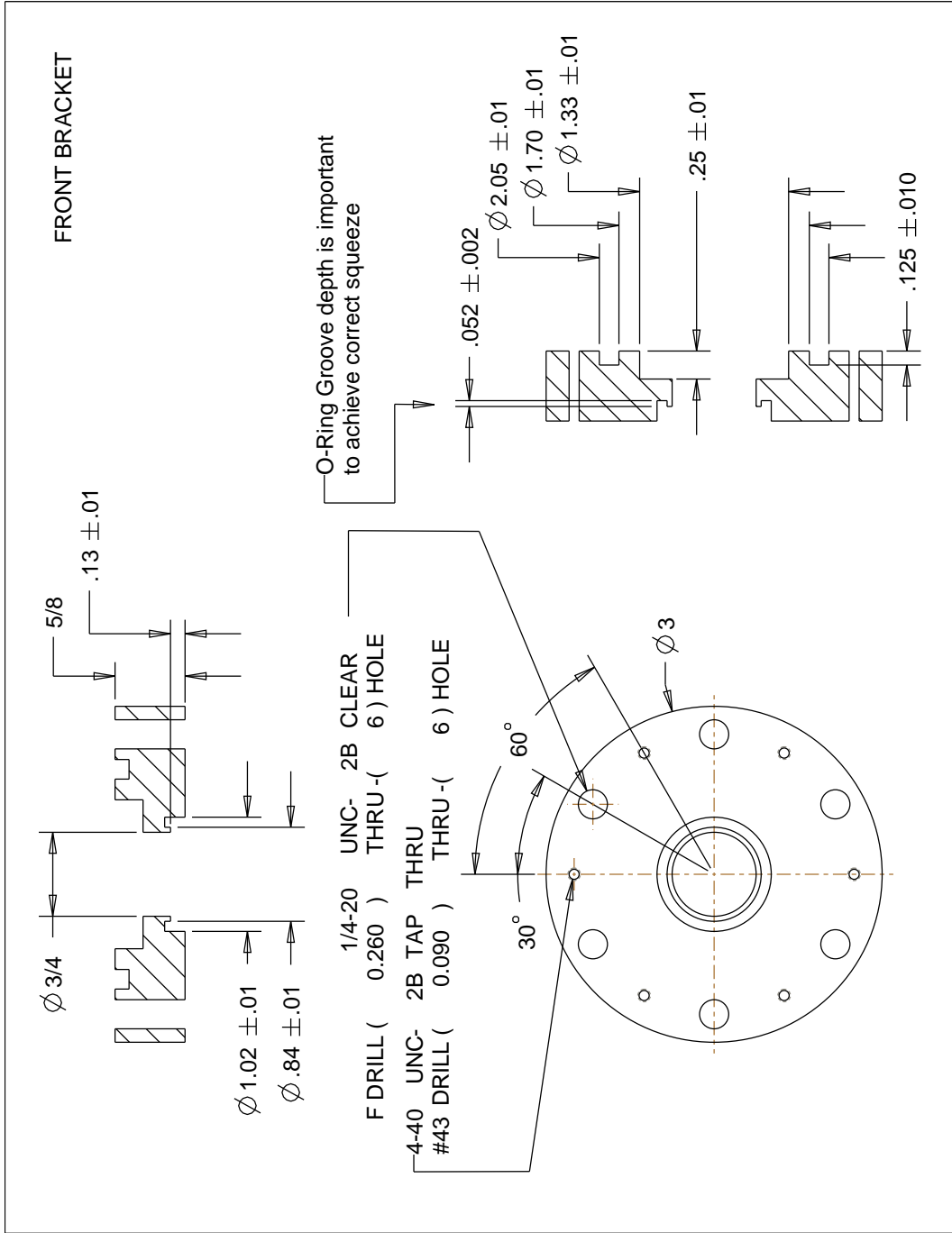


Figure A-3-2: Front bracket.

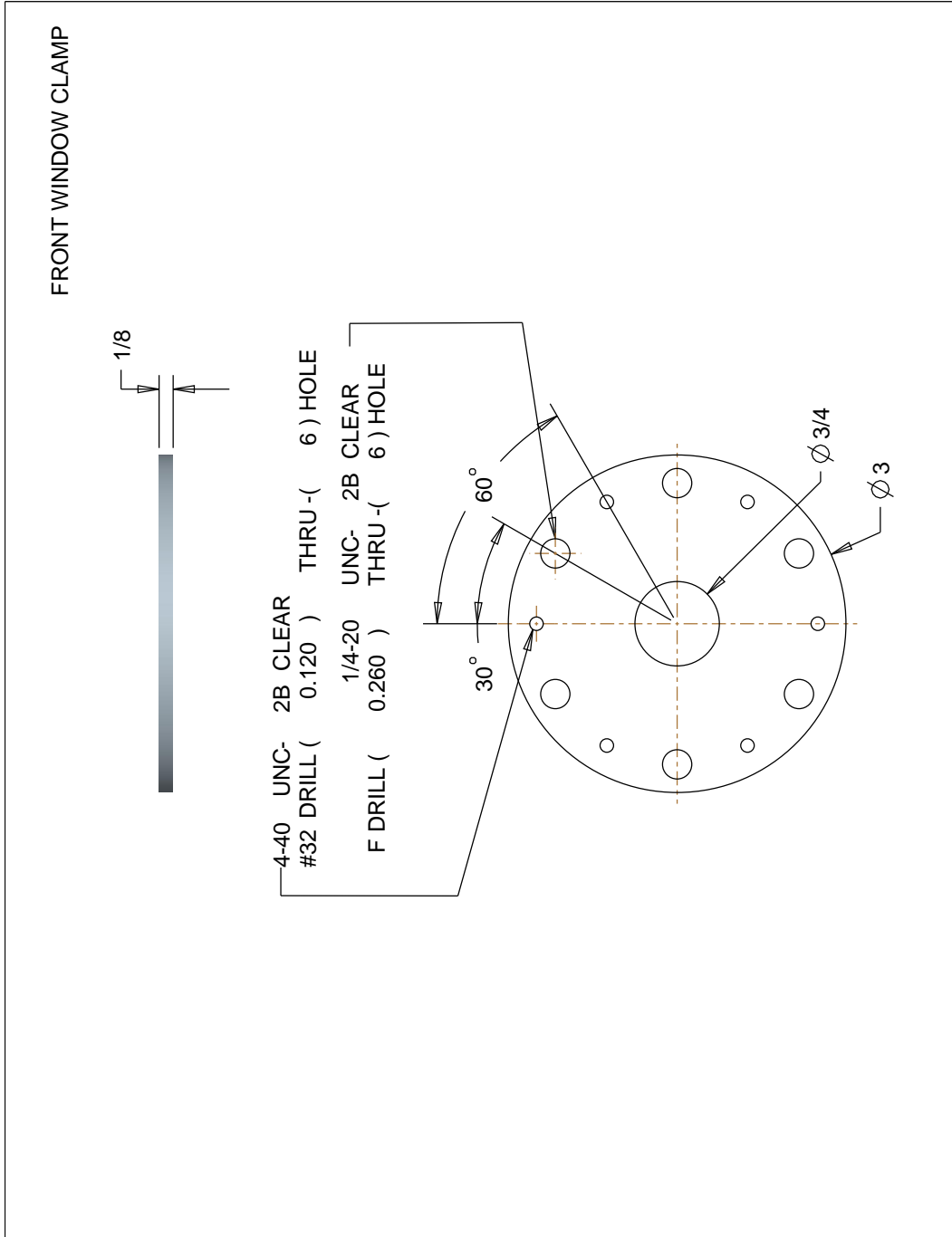


Figure A-3.3: Front window clamp.

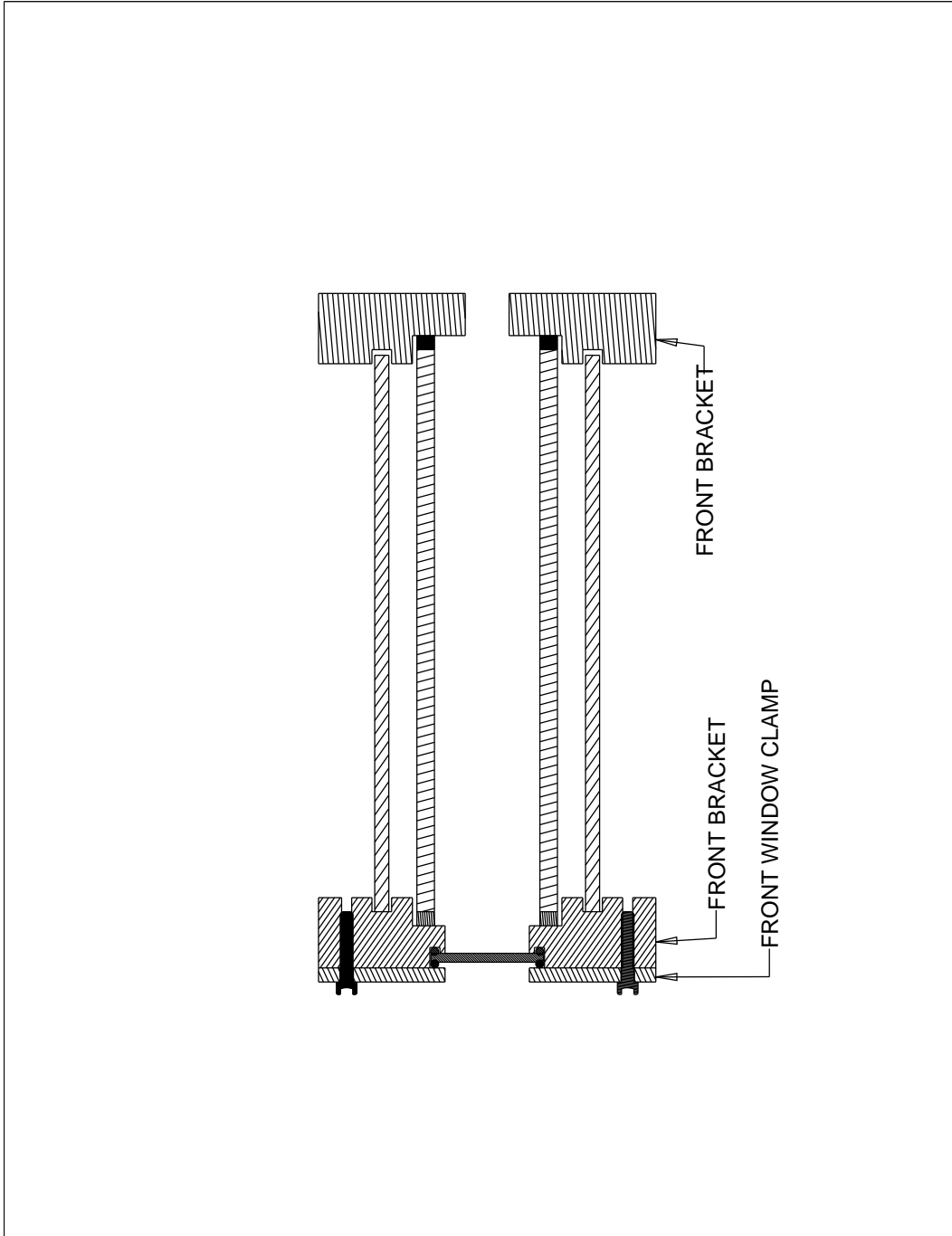
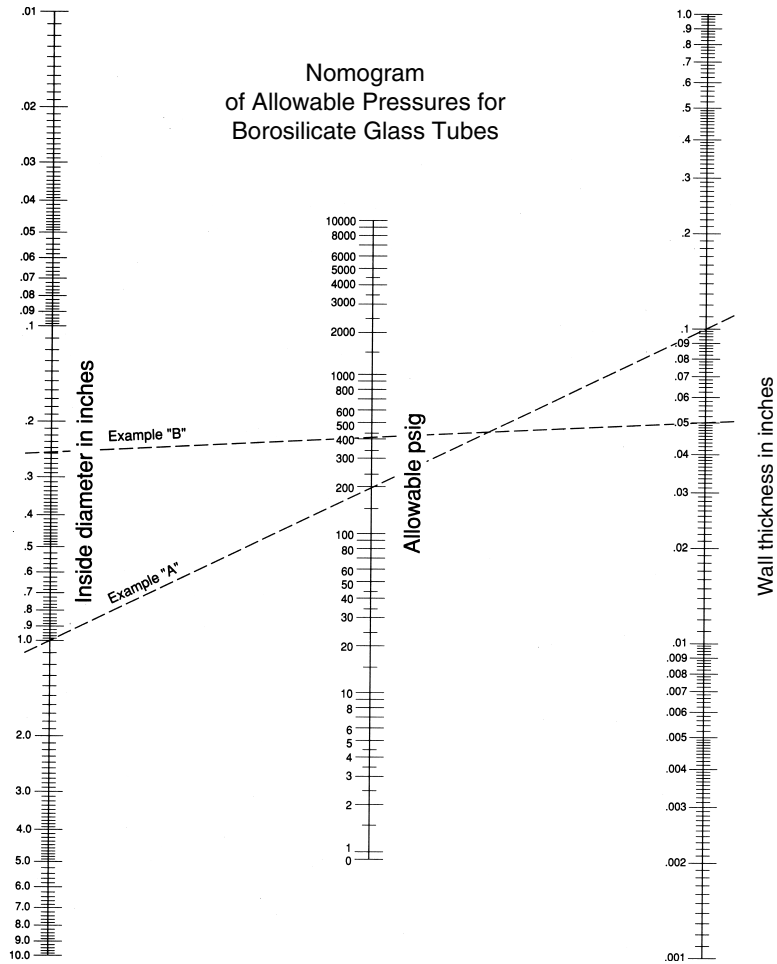


Figure A-3.4: Assembled pressure chamber cross-section.

**TECHNICAL INFORMATION:
 Nomogram of Allowable Pressures**



CAUTION: With any glassware used for pressure or vacuum applications, great care must be taken in handling. The strength of the glass can be degraded due to scratches, checks and abrasions. Always use protective shielding and eyewear when working with glass under pressure.

Figure A-3.5: Nomogram used to find minimum safe wall thickness of pressure chamber tube.